Russian Chemical Reviews **67** (5) 357 – 374 (1998) © 1998 Russian Academy of Sciences and Turpion Ltd

UDC 541.16

Intermetallic borocarbides: electronic structure, chemical bonding, and properties

A L Ivanovskii

Contents

I.	Introduction	357
II.	Phase relationships in Ln – M – B – C systems	358
III.	Electronic structure of nonmagnetic superconductors $LuNi_2B_2C$ and YNi_2B_2C	359
IV.	Chemical bonding in intermetallic borocarbides	361
V.	The effect of the composition of metal and metalloid sublattices on the energy band structure of the LnM_2B_2C phases and their solid solutions	362
VI.	The energy band structure of 'two-layered' LnNiBC borocarbides and solid solutions based on them	366
VII.	Electronic structure and some physicochemical properties of intermetallic borocarbides	367
VIII.	Spectroscopic studies of the electronic structure of intermetallic borocarbides	370
IX.	Conclusion	372

Abstract. In 1994, the superconductivity of intermetallic borocarbides (IBC) of composition LnM_2B_2C, where Ln is a rare-earth metal and M is Ni or Pd, was discovered. This discovery stimulated numerous works on the synthesis of new quaternary borocarbide phases and solid solutions based on them and studies of their crystal chemistry and magnetic, superconducting, and transport properties. Almost simultaneously, investigations of the fundamental electronic properties of IBC and specific chemical bonding in this new class of materials have been initiated. The results of theoretical and experimental investigations in these fields are summarised. The bibliography includes 179 references.

I. Introduction

The year 1994 was marked by a discovery in the physical chemistry of a poorly studied class of multicomponent intermetallic compounds, *viz*., intermetallic borocarbides (IBC): the superconductivity effect was observed in the Y – Pd – B – C and Lu – Ni – B – C systems. Superconducting transitions at $T_c \approx 23$ K and $T_c \approx 16$ K for a heterophase specimen with the composition $YPd_5B_3C_{0.3}$ and a single-phase specimen of borocarbide $LuNi_2B_2C$, respectively, were reported.[13]

The attention of researchers was immediately drawn to IBC since they appeared to be the first superconducting quaternary intermetallic systems known which are devoid of copper and oxygen ions. The above phases had nickel and palladium as components. At the same time, it was well known that the presence of ferromagnetic nickel in compounds resulted in suppression of their superconducting properties, whereas very few superconductors studied contained appreciable quantities of palladium (for instance, PdH_x, metallic palladium saturated with boron and carbon ions, and several hydrogenated Pd alloys with *d*-metals (Cu, Ag, Au, Nb, Mo, and W).[4]

A L Ivanovskii Institute of Solid State Chemistry, Ural Branch of the Russian Academy of Sciences, Pervomaiskaya ul. 91, 620219 Ekaterinburg, Russian Federation. Fax (7-343) 274 44 95. Tel. (7-343) 249 30 82

Received 23 July 1997
Uspekhi Khimii **67** (5) 403 – 422 (1998); translated by A M Raevsky

The observation of superconductivity in nickel-containing IBC stimulated an active search for other multicomponent phases containing magnetic transition-metal ions. Currently, information on the synthesis of superconducting intermetallic silicides and carbides, namely, LaNiSi, $LaNiC_2$, $La_{1-x}Th_xNiC_2$, and $Tm_2Fe_3Si_5$ is available.[5 – 8]

The initial stage of experimental studies of IBC was characterised by a quest to extend the class of known quaternary phases of the $LuNi_2B_2C$ type by replacing Lu by magnetic rare-earth metal ions and to determine the critical temperature of superconducting transition (T_c) for compounds produced. This kind of study was carried out for IBC containing Tm ($T_c \approx 10.8$ K), Er ($T_c \approx 10.5$ K), Ho ($T_c \approx 8.5$ K), and Dy ($T_c \approx 6.2$ K).[9 – 14] Similar attempts to 'chemically modify' the superconducting properties were made by changing the type of the transition metal. In particular, it has been established that for YNi_2B_2C ($T_c \approx 15.6$ K)[2] such substitutions appreciably affect the T_c value, which is equal to 10.0, 23.0, and 0.0 K for Pt,[15] Pd,[16, 17] and Co,[18] respectively.

One more remarkable discovery was made at the same period. It has been established in studies of the properties of IBC containing magnetic rare-earth metal ions (Pr, Dy, Ho, Er, Tb, *etc*.)[19 – 25] that these compounds form a unique class of superconducting materials with close-lying temperatures of magnetic ordering, namely, the Neel temperature (T_N) and the temperature of superconducting transition. In this regard, no other analogues of IBC are known so far.

The current stage of investigations of IBC is characterised by both a search for new quaternary phases, in which the metallic sublattice is composed of actinides [for instance, phases in the UMBC systems (M = Ni, Pd, and Pt)],[26 – 29] and attempts to synthesise intermetallic boron nitrides[30, 31] as well as by a tendency to perform more flexible variation of the composition and properties of IBC by doping their sublattices with a finite (variable) concentration of dopants. Transition metals (M′), as a rule, play the role of dopants. The concentration dependences of physicochemical characteristics of solid solutions (SS) of the type $Ln(M_{1-x}M'_x)_2B_2C$[32 – 35] or $Ln(M_{1-x}M'_x)BC$[36, 37] are being studied intensively. Thermobarochemistry techniques are also used to affect the crystal structure.[36] Attention is focused on the effect of possible processing conditions (for instance, annealing) on the properties of the specimens. On the whole, the majority of

experiments deal with the studies of the nature of superconducting, magnetic, and kinetic properties of IBC and the ways of their targeted control.

Each group of superconducting materials [high-temperature superconducting (HTSC) cuprates, fullerites, Chevreul's phases, A-15 compounds, *etc*.] is characterised by its individual crystal structure and the structure of the energy bands. Therefore, it is natural that a set of experiments on studying the specific character of the electron states in IBC were initiated almost simultaneously with the discovery of superconductivity in borocarbide phases.

The information on the electronic energy spectra (EES) and the nature of chemical bonding in IBC obtained to date using computational methods of solid state quantum chemistry and experimental spectroscopic techniques is analysed in the present review. Attempts aimed at interpreting the observed physicochemical properties of IBC from the viewpoint of their electronic structure are considered.

II. Phase relationships in Ln – M – B – C systems

No detailed studies of phase equilibria in Ln – M – B – C systems have been reported to date; information on phase relationships in these systems and plausible structures of compounds that formed is scarce and is of tentative character so far.[38]

In the first papers,[13] the $LuNi_2B_2C$, YNi_2B_2C, and YPd_2B_2C phases as well as the related LuNiBC phase were identified as superconducting ones. The efforts of chemists were focused on obtaining a series of isostructural compounds in analogous systems. To date, the $LnNi_2B_2C$ phases for most 4*f*-elements, Y, and Sc have been synthesised.[1–3,9–14,39,40] Substances obtained by complete substitution of Ni by Pd, Pt, Rh, or Ir appear to be thermodynamically stable only for early lanthanides.[1,15,40] As to borocarbides with the composition LnMBC, the attempts to synthesise isostructural phases corresponding to various combinations of rare-earth and transition metals made it possible to establish reliably the existence of only borocarbides LuNiBC and YNiBC, whereas the attempts aimed at obtaining stable single-phase specimens with La, Ce, Ni, Co, and Cu failed.[9,36,41,42]

The crystal structure of the borocarbides $LuNi_2B_2C$ and LuNiBC was first studied by Schmidt *et al*.[9] The fragments of these structures are shown in Fig. 1 and some of the crystallographic parameters are listed in Table 1. The structure of $LuNi_2B_2C$ can be considered as a modified 'filled' variant of the body-centred tetragonal (BCT) structure of the $ThCr_2Si_2$ type (see Ref. 38) with the space group $I4/mmm$ composed of alternating Ni_2B_2 layers (with tetrahedral coordination of Ni atoms) and plane LuC nets, where the atomic ordering is of the rock salt type.

The Ni_2B_2 layers in LuNiBC borocarbide are separated by two LuC nets; however, several interatomic distances appear to be very close for both phases (see Table 1).

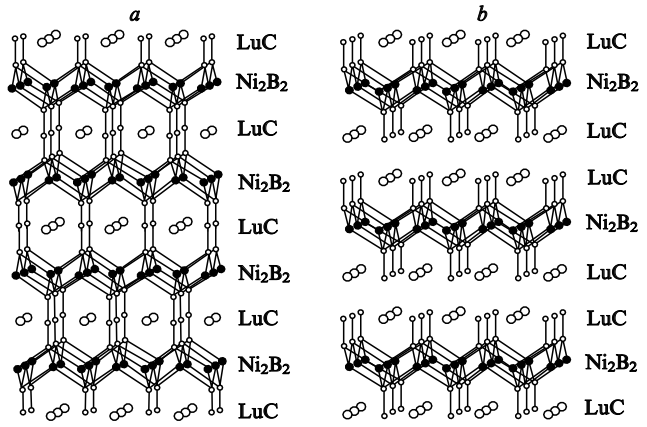


Figure 1. The crystal structures of borocarbides.[9] (*a*) $LuNi_2B_2C$; (*b*) LuNiBC.

Table 1. Crystallographic parameters of $LuNi_2B_2C$ and LuNiBC.

Parameter	$LuNi_2B_2C$	LuNiBC
Symmetry group	$I4/mmm$	$P4/nmm$
Unit cell parameter /Å		
a	3.4639	3.4985
c	10.6313	7.7556
Unit cell volume /Å^3	127.56	94.93
The number of formula units per unit cell	2	2
Atomic *x*, *y*, *z* positions of the element		
Lu	0, 0, 0	1/4, 1/4, 0.1602
Ni	1/2, 0, 1/4	3/4, 1/4, 1/2
B	0, 0, 0.3621	3/4, 3/4, 0.1523
C	1/2, 1/2, 0	3/4, 3/4, 0.3489
Interatomic distance /Å		
Lu – C	2.449	2.475
Lu – B	2.855	2.867
Ni – B	2.10	2.11
Ni – Ni	2.449	2.474
B – C	1.47	1.52

In accordance with the classification suggested by Gangopadhyay *et al*.,[37] the LnM_2B_2C phases have the simplest (for this series of compounds) structure with alternating M_2B_2 and LnC layers (the so-called 'one-layered' phases) and can be described by the general formula $(LnC)_n(MB)_m$, where $n = 1$, and $m = 2$. Compounds with the composition LnMBC belong to the 'two-layered' phases ($n = 2$, $m = 2$). Schmidt *et al*.[9] and Gangopadhyay *et al*.[37] assumed that the systems in question may exist as extended homologous series with the compositions $(LnC)_n(MB)_2$ and $(LnC)(MB)_{m+2}$ with variable content of the nets of the LnC and M_2B_2 phases, respectively, and their combination, the $(LnC)_n(MB)_{m+2}$ phase. No experimental confirmations of the existence of such compounds are available to date.

Analysis of the structure of the $LnNi_2B_2C$ phases has shown[9] that the constants *a* and *c* of the BCT lattice change almost linearly depending on the lanthanide radius *r*(Ln)[43,44] (Fig. 2) in contrast to the expected effect of conventional lanthanide compression according to Vegard's rule. The only exception is $CeNi_2B_2C$, which is explained by variable (or mixed) valence of cerium ($Ce \sim 3.75$) due to hybridisation of its 4*f* shell with the states of the valence band of the crystal.[45–47]

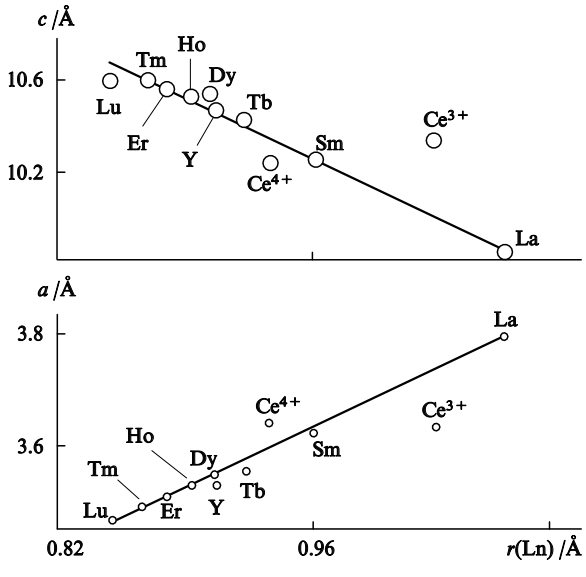


Figure 2. Dependence of the BCT lattice parameters of $LnNi_2B_2C$ phases on the ionic radius of the lanthanide.

Table 2. Structural parameters of the $LnNi_2B_2C$ phases.[47]

Parameter	$CeNi_2B_2C$	$PrNi_2B_2C$	$NdNi_2B_2C$	$TbNi_2B_2C$	$DyNi_2B_2C$	$HoNi_2B_2C$	$ErNi_2B_2C$	$TmNi_2B_2C$	$YbNi_2B_2C$
a /Å	3.638	3.707	3.678	3.554	3.534	3.513	3.502	3.487	3.478
c /Å	10.227	9.999	10.081	10.435	10.488	10.528	10.558	10.586	10.607
V /Å^3	135.346	137.383	136.370	131.778	130.999	130.271	129.48	128.682	128.323
Lu – B /Å	2.972	3.012	2.995	2.921	2.907	2.896	2.885	2.888	2.877
Lu – C /Å	2.572	2.621	2.601	2.512	2.499	2.487	2.476	2.469	2.459
Ni – B /Å	2.109	2.113	2.111	2.101	2.101	2.101	2.100	2.095	2.091
B – C /Å	1.489	1.489	1.485	1.489	1.485	1.483	1.481	1.485	1.483
B_i – Ni – B_{ii} /deg	104.85	103.33	103.93	106.53	107.02	107.41	107.74	107.92	107.92
B_i – Ni – B_i /deg	119.16	122.61	121.25	115.55	114.51	113.69	113.03	112.64	112.64

Note. Atomic positions in the unit cell: Ln (0, 0, 0), Ni (1/2, 0, 1/4), B (0, 0, z), C (1/2, 1/2, 0), B_i (x, y, z), B_{ii} (1/2 + x, 1/2 + y, 1/2 – z).

The most detailed study of crystallochemical properties of the $LnNi_2B_2C$ (Ln = Y, Ce, Pr, Nd, Tb, Dy, Ho, Er, Tm, and Yb) phases (Table 2) was carried out by the neutron diffraction technique.[47] The interatomic Ln – C and Ln – B distances increase appreciably with the lanthanide radius, which results in a decrease in the thickness of the Ni_2B_2 layer and distortion of NiB_4 tetrahedra it is composed of. Since the Ni – B distances are little changed, the most pronounced changes occur in the bond angles of the NiB_4 fragments (Table 2). The interatomic B – C distances appear to be the least 'sensitive' to the r(Ln) values, which is explained[47] by the strongest interspecies interactions in the C – B – C groups (see below).

It should be noted that the strongly anisotropic quasi-two-dimensional (2D) structure of IBC can indicate at first glance the similarity in the nature and mechanism of superconductivity in these phases and in 2D high-temperature superconducting cuprates. Such a similarity seems to be real, in particular, taking into account the assumptions by Disalvo[48] and Geballe[49] that partial replacement of copper atoms in cuprates by atoms of other transition metals and that of oxygen atoms by more electropositive ions (N, C, B) can be considered in several cases as the factor that prognostically favours superconductivity. However, it should be immediately noted that all information concerning the specificity of the electronic structure of IBC available to date rules out the possibility of the above analogy.

III. Electronic structure of nonmagnetic superconductors $LuNi_2B_2C$ and YNi_2B_2C

The first numerical calculation of the electron states of $LuNi_2B_2C$ was carried out by Mattheiss[50] in the framework of the local electron density formalism (LEDF) by using the scalar relativistic linearised augmented plane waves (LAPW) method.[51, 52] The exchange-correlation effects were taken into account by the use of Wigner's interpolation formula.[53]

The dispersion dependences $E(\boldsymbol{k})$ are shown in Fig. 3. The lowest energy band is formed by the C2s states. The allowed states in the interval from -10 eV to the Fermi level are composed of contributions of the B2s, B2p – C2p, and Ni3d states (in order of increasing energy). The Fermi level cuts the Ni3d bands partially 'seizing' the bottom of the Lu($d_{x^2-y^2}$) subband (at the point Γ). The major contribution to the maximum near the Fermi level [$N(E_F)$] comes from the Ni3d states: 2.4 states per eV for a transition metal, which is approximately twice as large as the corresponding value for copper in the case of HTSC cuprate La_2CuO_4 (see Ref. 54) and is close to $N(E_F)$ for vanadium in the 'conventional' A-15 superconductor V_3Si.[55] Hence, Mattheiss[50] has come to the conclusion that $LuNi_2B_2C$ must be considered as a 'conventional' superconductor with the known T_c *vs.* $N(E_F)$ (or T_c *vs.* γ, where γ is the electronic heat capacity) dependence.[56]

Experimental measurements of γ for $LuNi_2B_2C$ and $LaPt_{1.7}Au_{0.3}B_2C$ have been performed[57] almost simultaneously with Mattheiss' calculations,[50] with γ values being close to those of A-15 compounds.

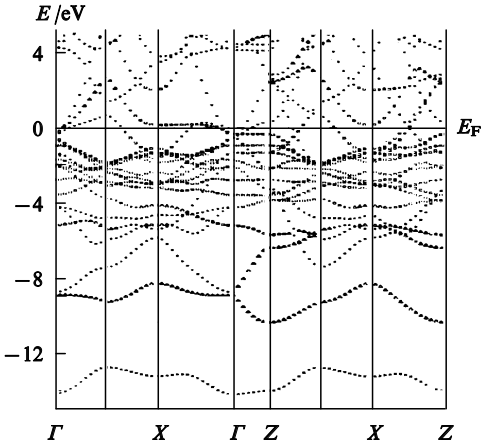


Figure 3. The band structure of $LuNi_2B_2C$.[50]

Analysis of the distribution of the valence s, p, and d states of lutetium (Fig. 4) shows[50] that their contributions to the formation of $N(E_F)$ cannot be neglected, in contrast, for instance, to the case of HTSC lanthanum cuprate.[54] The near-Fermi region of the spectrum of $LuNi_2B_2C$ contains all five Ni3d subbands.[50] The contributions of the d_{xy} and $d_{yz,zx}$ states to $N(E_F)$ exceed those of the $d_{x^2-y^2}$ and $d_{3z^2-r^2}$ states only by 16% and 6%, respectively. The inclusion of Lu 4f levels into the valence basis set has nearly no effect on the shape of the curve of the total density of states (TDOS). In this case, the shapes of TDOS for $LuNi_2B_2C$ and YNi_2B_2C appear to be similar (Fig. 4). The latter was calculated by Schmidt *et al.*[9] using the values 3.53 and 10.57 Å for the lattice parameters a and c, respectively.

Judging from the results obtained, the energy-band spectra of Lu and Y borocarbides do not satisfy the criterion for that of promising HTSC phases,[58] which requires that the σ^* band formed as a result of interaction between the degenerate anionic and cationic levels be half-filled. Unlike cuprates, where the corresponding bands are in the immediate vicinity of E_F, the Ni3d – B2s or Ni3d – C2p bands of borocarbides have different energetics owing to a specific character of interatomic σ-bonds in the NiB_4 tetrahedra.

Data on the energy band structure of $LuNi_2B_2C$ obtained by the LAPW method[59] in the LEDF parametrisation[60–63] using the lattice constants a = 3.464 Å and c = 10.631 Å, and z/c = 0.1379, where z characterises the position of the B atoms above the Lu – C plane, coincide in general with those obtained by Mattheiss *et al.*[58, 64] The shape of the Fermi surface determined by Pickett *et al.*[59] appeared to be rather complicated: the Lud and Nid – B2p type spheroids that form the Fermi surface are centred at the centre of the Brillouin zone. The fact that the dispersion of the

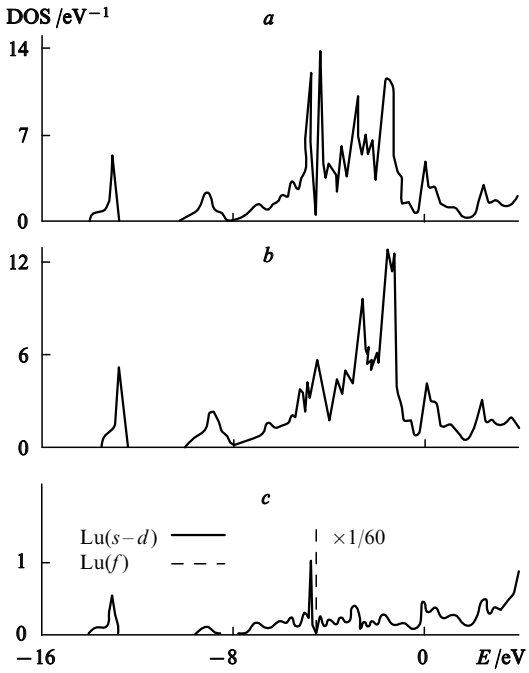


Figure 4. The energy distribution of the total densities of states for $LuNi_2B_2C$ (*a*), YNi_2B_2C (*b*), and partial ($s-f$) Lu states in $LuNi_2B_2C$ (*c*); calculations by the LAPW method.[50]

corresponding energy bands is comparable in the atomic planes and along the *c* axis, as is the case in Mattheiss' calculations,[50] is an unambiguous evidence for the three-dimensional (3*D*) nature of the electronic energy spectra of IBC.

Particular attention was given to the analysis of the structure of bands near the Fermi level responsible for the formation of the DOS maximum at the Fermi level. Its presence is associated with the formation of plane energy bands in the (110) direction (the $\Gamma-X$ direction in Fig. 3), which include antibonding (Nid_{z^2} – Nid_{z^2}), bonding (Bp – Nid), and impurity (Lu$d_{xz,yz}$) states. Taking into account an appreciable contribution of the Ni*d* states to $N(E_F)$, one can assume that (by analogy with the known ferromagnetic behaviour of metallic nickel or nickel films) this peak in IBC is unstable according to Stoner. However, no ferromagnetic instability of this type was shown in calculations [59] carried out with consideration of the spin moments.[65,66]

Pickett *et al.*[59] emphasised that the appearance of the near-Fermi 3*d*-like band of Ni separated from all the other filled Ni*d* bands is one of the most remarkable features of the $LuNi_2B_2C$ electronic spectrum and studied its genesis in detail. To this end, the sublattices of the 'empty' BCT phase were progressively 'filled' with the corresponding atoms. Calculations of isolated Ni and Ni_2B_2 monolayers that retained their atomic geometry in the bulk of $LuNi_2B_2C$ did not result in splitting of the Ni*d* subband; only the addition of bridging carbon atoms made it possible to detect a resonance DOS peak of the Ni3*d* type separated from the main *d* band of nickel. However, the energetics and structure of the near-Fermi maximum characteristic of a superconducting IBC is formed finally in the presence of the Lu atoms, *i.e.*, when Ni – C interactions are corrected taking account of the carbon – lutetium bonds.

Such analysis not only confirms the 3*D* nature of IBC,† but is of importance from the viewpoint of methodology. It shows that the local models that take into account only the closest environment of the transition-metal atom cannot be used for interpreting the superconductivity effects in IBC, which was the usual practice in the first stages of the description of electronic energy spectra of HTSC cuprates (for a review, see Ref. 67). Therefore, one should be extremely careful when applying cluster quantum-chemical methods to the class of intermetallic borocarbides; in particular, the chosen fragments must be balanced with respect to the stoichiometric composition of real IBC materials. Analogous conclusion was drawn by Kim *et al.*[68] who have calculated the energy band structure of $LuNi_2B_2C$ by the *ab initio* pseudopotential method.[69]

The energy band structure of the BCT borocarbide YNi_2B_2C was studied by Mattheiss,[50] Coehoorn,[70] Lee *et al.*,[71] Ravindran *et al.*,[72] and Zeng *et al.*[73] The dispersion dependences $E(\boldsymbol{k})$ and DOS distributions for the YNi_2B_2C phase found by these authors are in good agreement with each other despite certain deviations in numerical estimates of EES inevitable if different methods and approximations are used for the accepted models. For this reason, the results obtained by Lee *et al.*[71] will be used in the subsequent description of characteristic features of the electronic structure of YNi_2B_2C. The calculations were performed by the self-consistent linearised muffin-tin orbital (LMTO) method with the lattice parameters $a = 3.527$ Å and $c = 10.5427$ Å.[74]

The structure of the energy bands of YNi_2B_2C is shown in Fig. 5, several parameters of the electron states are listed in Table 3. Lee *et al.*[71] draw attention to the composition of the bands near the Fermi level, which consist mainly of the Ni3*d* contributions and appreciable admixtures of the Y4*d*, B2*p*, and C2*p* states. The flat band crossed by the Fermi level at the point Γ results in the appearance of the van Hove-like singularity on the TDOS curve. Cross-section of the Fermi surface by the $k_z = 0$ plane of the Brillouin zone is shown in Fig. 6. Its topology (see Fig. 5) is formed with participation of the bands that determine the combination of the electron and hole states. An appreciable energy dispersion of the C2*p*-like bands in the $\Gamma-Z$ direction was noted.[71] It was also emphasised that it is carbon that plays the crucial role in the formation of the 3*D* nature of the given phase, whereas a quasi-2*D* behaviour is expected for a hypothetical IBC with an 'empty' C sublattice.

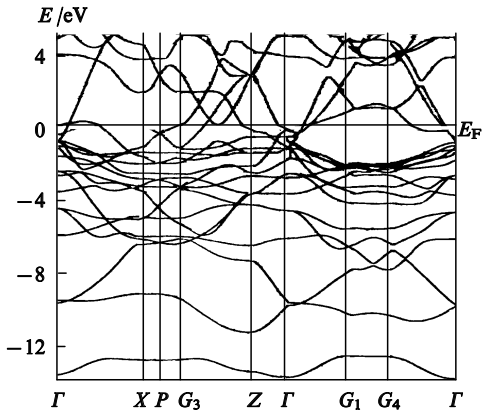


Figure 5. The band structure of YNi_2B_2C calculations by the LMTO method.[71]

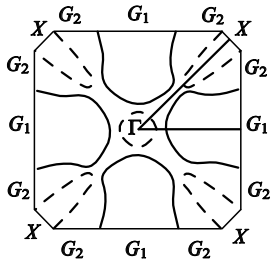


Figure 6. Cross-section of the Fermi surface of BCT YNi_2B_2C by the $k_z = 0$ plane.[71]

† The states of all of the atoms that constitute the material are involved in the formation of subtle features of the near-Fermi interval of the energy band spectrum responsible for superconductivity of 3*D* IBC.

Table 3. Contributions of individual states ($N_{s,p,d}$) to the DOS at the Fermi level, charges ($Q_{s,p,d}$) of the 'muffin-tin' spheres for individual atoms in the YNi_2B_2C phase, and radii of atomic spheres (R); calculations by the LMTO method.

Parameter	Y	Ni	B	C
N_s /state per 1 eV	0.02	0.03	0.04	0.03
N_p /state per 1 eV	0.07	0.22	0.18	0.14
N_d /state per 1 eV	0.64	1.09	–	–
N_{s+p+d} /state per 1 eV	0.73	1.34	0.22	0.17
Q_s /e	0.58	0.67	0.86	1.08
Q_p /e	1.18	0.87	1.58	2.48
Q_d /e	2.37	8.86	–	–
Q_{s+p+d} /e	4.13	10.22	2.44	3.56
R /a.u.	3.36	2.55	1.97	1.94

The nature of chemical bonding in IBC has not been analysed in detail.[50, 59, 64, 68, 70–73] Certain qualitative conclusions on the dominance of one or another type of interaction were based on the energy distributions of the local densities of states (LDOS) considered in Refs 75 and 76.

IV. Chemical bonding in intermetallic borocarbides

The nature of the formation of chemical bonds in IBC and the role of particular atoms and atomic groups were considered by Zeng *et al.*[73] and Halet.[77] The main attention was given to calculations of the indices of local interatomic interactions such as the overlap integrals (OI) of effective atomic orbitals.

A semiquantitative analysis of chemical bonding for $LuNi_2B_2C$ was performed by Halet[77] in the framework of the tight-binding method,[78, 79] which is the energy-band version of the extended Hückel method.

The molecular orbital (MO) diagram of the isolated B_2C^{2-} group (Fig. 7) illustrates the character of the interaction between the boron and carbon atoms, which form the corresponding sublattices in IBC. Hybridisation of 2*s* and 2*p* atomic orbitals (AOs) of the B and C atoms results in the formation of six σ-type MOs, two of which are bonding, two are nonbonding (σ_g and σ_u), and two are of pronounced antibonding nature. In addition, the MO system includes degenerate π-type orbitals corresponding to bonding ($1\pi_u$), nonbonding (π_g), and antibonding ($2\pi_u$) interactions of the $p-p$ states.

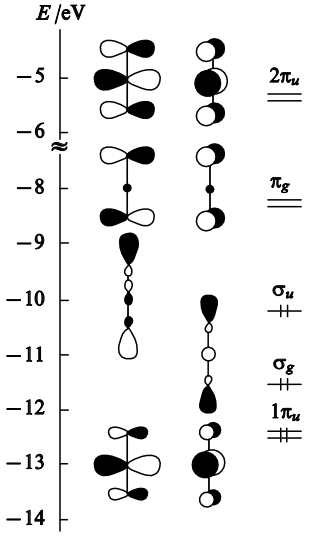


Figure 7. The molecular orbital (MO) diagram of $(B_2C)^{2-}$ group for an IBC with the BCT structure of the $ThCr_2Si_2$ type.

The energy interval (the 'forbidden gap') between the highest nonbonding (π_g) and the lowest antibonding ($2\pi_u$) MO depends[77] on the formal charge ascribed to the B_2C group and diminishes sharply on going from $(B_2C)^{3-}$ to $(B_2C)^{2-}$. The subsequent decrease in the 'forbidden gap', which is absent in a real IBC material, is associated with the formation of metal–nonmetal covalent interactions.

Numerical estimates of OI and effective atomic charges (q_{ef}) are listed in Table 4. Interactions of a complex, ionic-covalent type, which differ considerably for particular intervals of the energy spectrum, have been found in IBC. In particular, the hybridised σ-bonding $Ni-B_2C$ states and the nonbonding (π_g and σ_u) states of the B_2C group with admixture of the antibonding π states of $Lu-C$ participate in the formation of states near the Fermi level.

Table 4. Overlap integrals (OI) and effective charges (q_{ef}) of the atoms and groups in $LuNi_2B_2C$.

Atomic pair	OI /e	Atom, group	q_{ef} /e
Ni – Ni	0.138	Lu	+1.48
Ni – B	0.304	Ni	−0.50
B – C	1.023	B	+0.35
Lu – B	0.072	C	−1.18
Lu – C	0.157	B_2C	−0.48

Zeng *et al.*[73] discussed the nature of the formation of individual interatomic bonds in YNi_2B_2C using the discrete variational[80–82] embedded-cluster approach in the framework of the local electron density functional. According to this model, the interaction between the chosen 71-atomic fragment $[Y_{12}Ni_{15}B_{32}C_{12}]$ with D_{2d} symmetry and the crystalline environment was calculated using a scheme developed by Ellis and coworkers.[83–85] The von Barth–Hedin exchange-correlation potential[86] was used, and the numerical basis set included the following AOs: 4*s*, 4*p*, 4*d*, 5*s*, and 5*p* of Y; 3*s*, 3*p*, 3*d*, 4*s*, and 4*p* of Ni; and 1*s*, 2*s*, and 2*p* of B and C.

The AO populations and OIs for this cluster in the YNi_2B_2C structure are listed in Table 5. According to these data, the metal and nonmetal atoms in YNi_2B_2C are in the cationic and anionic states, respectively, while the largest charge transfer is believed to occur in the plane nets from Y to C. As to the covalent component of the bond, the pair B – C bonds appear to be the most populated, as in $LuNi_2B_2C$. The Ni – B bonds are much less populated, whereas the Y – C interactions should be considered to be antibonding ones. It is clearly seen on the contour plots of the electron density distribution $\rho(r)$[73] that the electron density is concentrated along the lines of the Ni – Ni bonds (in the *xy* plane), that the bonding states are formed between the atomic Ni and Y layers, and that the interactions of the $Ni-B_2C$ type arise in the *yz* plane.

Table 5. Orbital populations, effective atomic charges, and overlap integrals for the 71-atomic cluster in the structure of YNi_2B_2C according to discrete variational calculations.

Atom	Orbital population			q_{ef}	Type of the bond	OI
	d	*s*	*p*			
Ni(1)[a]	9.06(3*d*)	0.38(4*s*)	0.52(4*p*)	+0.11	Ni(1) – B	0.64
Ni(2)[b]	9.11(3*d*)	0.41(4*s*)	0.39(4*p*)	+0.16	Ni(2) – B	0.66
Y	0.54(4*d*)	0.06(5*s*)	0.05(5*p*)	+2.49	Y – C	−0.18[c]
B		0.82(2*s*)	2.53(2*p*)	−0.35	B – C	1.14
C		1.40(2*s*)	4.35(2*p*)	−1.75		

[a] The central nickel atom in the cluster. [b] Peripheral nickel atoms in the cluster. [c] The 'minus' sign corresponds to antibonding.

V. The effect of the composition of metal and metalloid sublattices on the energy band structure of the LnM_2B_2C phases and their solid solutions

The study of the effect of the composition of metal and metalloid sublattices on the electronic energy spectra of IBC became a natural continuation of investigations into determination of the energy band structure of $LuNi_2B_2C$ and YNi_2B_2C, where either a complete replacement of one or several types of ions were by ions of another type was performed or a variable concentration of possible impurities was considered in the framework of the initial BCT structure.

1. Phases of composition LnM_2B_2C (M = Co, Cu, Pd, and Pt)

Mattheiss and co-workers [64] performed LAPW calculations of the EES for a series of BCT intermetallic borocarbides of composition $LnNi_2B_2C$ (Ln = La, Pr, Pm, ..., Tm, and Lu). The energy band structures of these IBC appeared to be similar to those of $LuNi_2B_2C$ and YNi_2B_2C discussed above. For all the phases under study, the valence band (of width $\sim$ 14 eV) contains 18 filled energy bands, including 10 Ni3*d* bands. The latter can be arbitrarily combined into two subbands located immediately near and below the Fermi level. Figure 8 presents the band structure of $LaNi_2B_2C$ as an example. For this phase, the free 4*f* states are localised $\sim$ 3–4 eV higher than E_F.

Special emphasis was placed by Mattheiss and co-workers [64] on the dispersion of the *sp* band (Γ_{2-}, indicated by the solid line in Fig. 8) near the Fermi level depending on the specific features of the structure of the individual phases, in particular, on the geometry of the NiB_4 tetrahedra. Calculations (in accordance with the experimental data discussed above) show that the lattice constants *a* and *c* in the $LnNi_2B_2C$ series change in different manner. A progressive distortion of the NiB_4 tetrahedra occurs with increase in radius of the lanthanide atom. Thus, the bond angles α change from 108.7° (Lu) to 102.1° (La), which results in the sharp (by $\sim$ 2 eV at the Γ point, see Fig. 8) change in the energetics and dispersion of the *sp* band and in a decrease in its contribution to the Brillouin zone and the degree of its filling. In turn, this affects the energy and character of filling of the Ni3*d* band (along the $\Gamma - X$ direction).

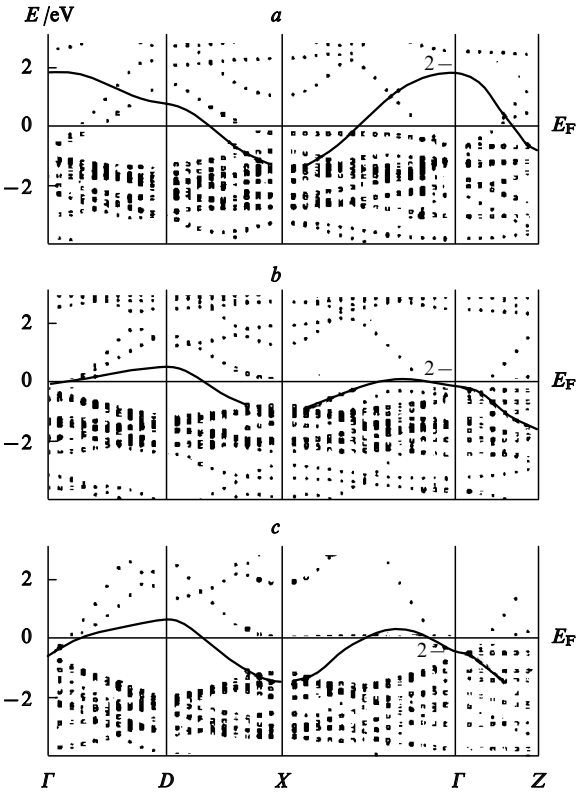


Figure 8. Dispersion of energy bands near the Fermi level for $LaNi_2B_2C$ (*a*), 'ideal' $LaNi_2B_2C$ (*b*), and $LuNi_2B_2C$ (*c*).
The band of nonmetal *sp* states near the Fermi level is indicated by solid line.

Mattheiss and co-workers [64] argue that these distinctions in subtle features of the energy distribution of the bands near the Fermi level are determined not by the type of the rearrangement of interatomic interactions resulting from the La → Lu substitution, but first and foremost by the structural factor, namely, by the degree of distortion of the NiB_4 tetrahedra, which increases with the lanthanide ionic radius. A trial calculation has been performed for a hypothetical 'ideal' compound $LaNi_2B_2C$ containing layers formed by regular NiB_4 tetrahedra (α = 109.5°, d(Ni–B) = 2.33 Å). Its band structure appeared to be close to that of $LuNi_2B_2C$ (α = 108.5°, d(Ni–B) = 2.11 Å). The $N(E_F)$ value for the 'ideal' $LaNi_2B_2C$ increases substantially (by $\sim$ 90%), thus approaching the $N(E_F)$ value for superconducting $LuNi_2B_2C$. It has been assumed [64] that the degree of distortion of the NiB_4 tetrahedra in the $LnNi_2B_2C$ phases as well as that of MB_4 tetrahedra (M = Pt, Pb, Ru, and Ir) in other known IBC can be deliberately controlled by using high-pressure techniques. In this case, the experiments on the hydrostatic or axial compression of IBC can result in revealing nontrivial T_c dependences on the lattice parameters for each particular material.

A comparative analysis of the energy band structure of $LuNi_2B_2C$ and $LaPt_2B_2C$ was carried out by Singh.[87] The energy spectra of these compounds calculated by the LAPW method were found to be similar. The distribution of the near-Fermi states has a pronounced 3*D* character and is close to an isotropic one, which means that the superconductivity of $LaPt_2B_2C$ ($T_c \simeq 11$ K) [40] can be considered in the framework of conventional Bardeen–Cooper–Schrieffer (BCS) mechanism by the analogy, for instance, with transition metal *B*1 carbides and nitrides.[88, 89] The main specific features of the energy spectrum of $LaPt_2B_2C$ are associated with the position of the flat Γ(110) band about 0.4 eV above the Fermi level. We remember that the corresponding band in $LuNi_2B_2C$ is in the immediate vicinity of the Fermi level and crosses it. As a result, the DOS maximum of the near-Fermi bands for $LaPt_2B_2C$ appears to be shifted toward the region of unfilled states. This leads to an appreciable decrease in $N(E_F)$ for $LaPt_2B_2C$ as compared to that for $LuNi_2B_2C$ despite the fact that the contributions of the *d* states of Ni and Pt to $N(E_F)$ for both phases are comparable in magnitude. Singh [87] explained the distinctions indicated above by the increase in the width of the Pt5*d* band (as compared to the Ni3*d* band) due to enhanced hybridisation of the platinum *d* states with metalloids (increased splitting of *d* states), which, in turn, is determined by greater extension of the *d* orbitals of Pt and La compared to those of Ni and Lu, respectively. Using the concepts of a relationship between T_c and $N(E_F)$ and the rigid band model,[4, 88, 89] Singh [87] assumed that an increase in the concentration of valence electrons (CVE), for instance, due to partial substitution of carbon atoms by those of more electronegative metalloids or the introduction of another 'electron donor' will have a favourable effect on the change of T_c of $LaPt_2B_2C$. For this phase, the optimum concentration of the 'excess' electrons, at which E_F coincides with the DOS maximum, is equal to $\sim$ 1.2 electrons per cell.[87]

Coehoorn [70] performed a detailed analysis of the composition of energy bands near the Fermi level for yet another representative of BCT borocarbides, *viz*., YPd_2B_2C, using the scalar relativistic version [69] of the augmented spherical waves (ASW) method. It was found for this compound that E_F coincides with the local DOS peak $N(E_F)$ = 3.26 eV^{-1} and the maximum contributions to $N(E_F)$ come from Pd4*d* and Y4*d* states (Table 6), as in nickel-containing Y and Lu borocarbides. It can be seen from the data in Table 6 that an appreciable filling of $d_{xz,yz}$ and d_{xy} orbitals occurs for yttrium and palladium, respectively. In the bulk of the crystal,

Table 6. Occupation numbers (state per 1 eV) of valence orbitals in the region $-0.2 \leqslant E_F \leqslant 0.2$ eV for YPd_2B_2C; calculations by the ASW method.

Atom	Occupation numbers							
	s	p_x, p_y	p_z	d_{xy}	$d_{xz,yz}$	$d_{3x^2-z^2}$	$d_{x^2-y^2}$	total value
Y	0.02	0.01	0.05	0.09	0.26	0.09	0.15	0.67
Pd	0.03	0.08	0.31	0.19	0.15	0.13	0.14	1.03
B	0.06	0.07	0.13	0.00	0.00	0.00	0.00	0.26
C	0.02	0.07	0.10	0.00	0.00	0.00	0.00	0.19

the Y atoms occupy the centre of the unit cell, the Pd atoms occupy positions (0, 1/2, 1/4) and (1/2, 0, 1/4); one of the 'blades' of the Y $d_{xz,yz}$ AOs is oriented along the Y–Pd bond, whereas the Pd4d_{xy} AOs are directed towards neighbouring Pd atoms. Considerable concentration of these states near E_F is due to their splitting into bonding and antibonding ones as a result of interatomic (and interlayer) interactions. This splitting is an additional indication of the 3*D* nature of the electron distributions in BCT intermetallic borocarbides.

Coehoorn [70] was the first who attempted to take into account the role of the magnetic order in the formation of energy spectra of IBC in ASW calculations of ferromagnetic $GdNi_2B_2C$. The major effect was the splitting of the DOS peak near the Fermi level by ~ 0.2 eV due to the direct intraatomic $4f-5d$ exchange interaction on Gd atoms. In the first approximation, the exchange splitting for all ferromagnetic compounds $LnNi_2B_2C$ is assumed to be proportional to the local magnetic moment. Then, the magnitude of this splitting for each Ln atom will be much larger than the width of the superconducting energy gap, which can be estimated as $\Delta E \simeq 0.05$ eV for $LnNi_2B_2C$ in the framework of the BCS theory; this indicates that the superconductivity is only possible in the case of antiferromagnetic spin ordering.

With the aim of elucidating the tendencies in the filling of the near-Fermi states, Coehoorn [70] calculated hypothetical ideal BCT crystals $LuCo_2B_2C$, $LuCu_2B_2C$, and $LuCo_2B_2B$; the interatomic distances in the above compounds were assumed to be identical and equal to those for $LuNi_2B_2C$ ($a = 3.4639$ Å and $c = 10.6313$ Å). It was concluded on the basis of calculations that the rigid band model will give reasonable results for the description of $N(E_F)$ changes in the case of chemical modification of IBC composition.[70]

2. Phases of composition YNi_2B_2X (X = B, C, N, and O)

The effect of variable concentration of the valence electrons on the filling of the near-Fermi states and the position of the Fermi level for BCT intermetallic borocarbides due to substitution of carbon atoms by other atoms was considered using YNi_2B_2X as an example. Calculations of hypothetical YNi_2B_2B, YNi_2B_2N, and YNi_2B_2O phases were carried out by the LMTO method.

It was established [71] that the structure of valence bands is strongly dependent on the composition of the X sublattice. The binding energies of quasi-core X2*s* bands increase in the series B < C < N < O and are equal to 10, 13, 17, and 21 eV, respectively. The X2*p*-like subbands fall into a similar sequence on the energy scale. Lee *et al.*[71] paid the major attention to the relative position of E_F and the DOS maximum near the Fermi level. It was shown that the position of the Fermi level for X = B is lower, whereas that for 'boron oxide' and, especially, for 'boronitride' is higher than the maximum of the DOS peak. The obtained estimates of $N(E_F)$ for YNi_2B_2X are 1.7, 4.40, 2.8, and 1.0 states per eV for X = B, C, N, and O, respectively. Lee *et al.*[71] believe that this indicates the maximum superconductivity of the borocarbide.

Naturally, the assumptions accepted [71] (first of all, the identity of the lattice parameters for all phases) make it possible to consider the results obtained as purely qualitative ones, especially with account of the data on the substantial role of B–C interactions in the formation of the crystal structure of IBC (see above). Obviously, the formulation of the problem of simulation of the effect of doping the nonmetal IBC sublattice on their energy band structure and, all the more, on their properties requires performing correct calculations of the energy parameters for substitution processes of such kind, estimates of the stability of solid solutions formed, and direct calculations of the values of their lattice constants.

3. Substitution solid solutions of composition $Y(Ni_{1-x}M_x)_2B_2C$ (M = Fe, Co, Ru)

Specific features of the electronic structure of the 'ideal' quaternary BCT LnM_2B_2X phases depending on the composition of their sublattices were considered above. Corresponding sites in such sublattices were occupied by atoms of rare-earth or transition metals, or by 2*p* atoms of the same sort.

A much more subtle effect on the properties of IBC can be exerted in the case of partial substitution of the atoms of a sublattice by 'related' atoms of another sort with the formation of quinary (and more complex) substitution solid solutions.

The first calculations of similar systems were carried out by Zeng *et al.*[73] in 1996 in the framework of the embedded-cluster approach. Before turning our attention to the results of these calculations, let us briefly consider experimental studies of the properties of the solid solutions mentioned above, in which the parameters of electronic spectra of multicomponent alloys are discussed.

It has been shown in the first numerical calculations of IBC that the *d* states of transition-metal atom play the determining role in the formation of the near-Fermi band, whereas the DOS of the conduction electrons genetically related to the rare-earth ions is rather low. Hence, the doping effects of a transition-metal sublattice will be the most 'impressive'; for this reason, fairly well studied YNi_2B_2C and $LuNi_2B_2C$ phases were mainly used as matrices and 3*d* and 4*d* transition metals (Co, Cu, Fe, Rh, Pd, *etc.*) were used as dopants.

Schmidt and co-workers [90] have synthesised single-phase specimens of $Y(Ni_{1-x}Co_x)_2B_2C$ ($0 \leqslant x \leqslant 1$) and studied the T_c dependences of these alloys on the concentration of impurity (Co). It was established that a sharp decrease in T_c (from ~ 15 K for the original YNi_2B_2C to ~ 1.2 K for $x \simeq 0.2$) occurs with an increase in x. Coehoorn [70] and Lee *et al.*[71] explained this effect qualitatively within the framework of the rigid band model taking into account the results of band calculations for the matrix, where a decrease in CVE upon introduction of cobalt will induce a decrease in $N(E_F)$.

Another interpretation can be given from the viewpoint of Kaiser's theory of nonmagnetic resonance states.[91] According to this theory, the change in T_c should be correlated with the resonance scattering of the conduction electrons and Coulomb interaction between localised *d* states. In this case, the dependence of T_c on the concentration of impurity (x) can be written as follows:[92]

$$T_c(x) = T_c(0)\exp\left(-\frac{Ax}{1-Bx}\right),$$

where coefficients A and B are functions of the LDOS at the Fermi level for the matrix and impurity [$N_{im}(E_F)$], respectively, of the parameter of the electron–phonon interaction λ, and effective interatomic Coulomb repulsion U_{ef}. The experimental dependence of T_c can be reproduced if $U_{ef} = 0.09$ eV, $N_{im}(E_F) = 11.8$ states per eV atom spin, and the 'critical' concentration of impurity (20%) can be found taking $N_{im}(E_F) = 0.2$ states per eV atom spin and $\lambda = 2.6$ (see Ref. 59). The values of $N(E_F)$ and λ are close in order of magnitude to those of mixed $Lu_2(Fe_{1-x}Co)_3Si_5$ alloys.[93]

The effect of Ni substitution by Co and Cu on T_c of $Y(Ni_{1-x}M_x)_2B_2C$ was studied by Goldman *et al.*[18] The specimens synthesised contained $\sim 95\%$ of a BCT phase with small amounts of Y_5C_6, YB_2C_2, YNi_2, and Ni_3C. It has been noted that copper possessed limited solubility in the original borocarbide. The lattice parameters (the initial values $a = 3.526$ Å and $c = 10.538$ Å coincide with those found by Schmidt *et al.*[94] and

Chakoumakos *et al.*[95]) increase or decrease as copper and cobalt, respectively, are introduced as dopants into YNi_2B_2C.

The introduction of Co or Cu into YNi_2B_2C results in a decrease in T_c, the effect being more pronounced for Co ($dT_c/dx = -45$ K for Co and $dT_c/dx = -19$ K for Cu in the region $x \leqslant 0.2$). At high concentrations of dopants the dependence of T_c is affected by multiphase composition of the specimens synthesised.

Several possible reasons for such a strong difference in the dopant effect on T_c of the alloys have been considered, *viz.*, the presence of carbon vacancies; local magnetism of cobalt ions; 'asymmetry' of the shape of the near-Fermi $N(E)$ peak of the matrix, and, finally, the role of the electron–phonon interaction. The assumption of an appreciable concentration of carbon vacancies was based on the presence of a stable boride YCo_2B_2 phase (see Ref. 96). In this case, the number of carbon defects in $Y(Ni_{1-x}Co_x)_2B_2C$ must increase with temperature, and the lattice constants should be appropriately changed. However, annealing of borocarbide specimens did not result in noticeable changes in a and c.

The increased dT_c/dx value for Co can be due to its magnetic properties; however, special experiments [16, 90] indicate a nonmagnetic behaviour of Co. Therefore, a relationship between the $T_c(x)$ dependence and the parameters of its electronic spectrum and/or electron–phonon interaction is most probable.

As to the role of the electron states, it should be noted that according to calculations,[70–72] the E_F value for YNi_2B_2C coincides with the LDOS maximum, *i.e.*, the introduction of either Co or Cu will shift the E_F value along the energy scale favouring an increase in $N(E_F)$ and, correspondingly, suppression of superconductivity. However, the sharp (more than twofold) difference in the effect of Co and Cu impurities on T_c cannot be explained in this case. An attempt to explain the observed effect by the change in the constant of the electron–phonon interaction (λ) cannot be considered as sound, since in this case the 'loosening' of the crystal structure upon introduction of Cu (the increase in the lattice parameters of the solid solution) will determine the increase in λ, whereas the cobalt impurity will have an opposite effect on λ.

Despite the contradictions mentioned above, the experiment confirms directly the principal results of calculations,[70–72] namely, that E_F coincides with the DOS maximum, which indicates that any attempts to 'chemically modify' the borocarbide composition aimed at increasing its superconducting characteristics [18] are not promising.

Gangopadhyay *et al.*[34] and Hoellworth *et al.*[97] discussed the changes in $N(E_F)$ and the role of the electron–phonon interaction in the formation of superconducting properties of $YNi_{2-x}(Co, Cu)_xB_2C$ alloys taking into account the results of experimental investigations of magnetic susceptibility (χ)

$$\chi = \chi_P + \chi_L + \chi_{VV} + \chi_c + \chi_i = \chi_{intr} + \chi_{imp}\,, \qquad (1)$$

where χ_P, χ_L, χ_{VV}, and χ_c are the Pauli paramagnetic, diamagnetic (of conduction electrons), van Vleck, and diamagnetic (of core electrons) contributions, respectively; χ_i is the contribution of paramagnetic impurities; and χ_{intr} and χ_{imp} are the intrinsic and impurity susceptibilities, respectively.

Gangopadhyay *et al.*[34] discussed the role of χ_{intr} and χ_{imp} for YNi_2B_2C doped with cobalt and copper. Assuming that χ_{intr} is independent of temperature and χ_{imp} obeys the Curie–Weiss law, one can write

$$\chi(T) = \chi_{intr} + \frac{C}{T - T_K}\,. \qquad (2)$$

It turned out that this dependence is valid for a narrow temperature range (see also Refs 97, 98) and appreciably decreases as temperature increases. Similar $\chi(T)$ dependences were also found in the studies of poly- and mono-crystalline specimens of YNi_2B_2C.[99, 100]

Assuming that the contributions of the orbital paramagnetism and atomic core diamagnetism are constant, the observed [34] $\chi(T)$ dependence can be explained first of all by temperature changes in the Pauli paramagnetism of the conduction electrons χ_P resulting from either rearrangement of the band spectrum or spin fluctuations.[99, 100] The presence of antiferromagnetic spin fluctuations was postulated [101, 102] for YNi_2B_2C and $LuNi_2B_2C$ to account for abnormal temperature dependences of ^{11}B spin-lattice relaxation times and the Knight shift. In a more recent study,[100] the temperature dependence of the magnitude and the sign of χ_P has been interpreted on the basis of the electronic energy spectrum. The results of the experiments on neutron scattering,[21] NMR,[100] spin relaxation,[103] and heat capacity [104] also provide no information on spin fluctuations for YNi_2B_2C.

The dependence of T_c on the effective DOS calculated for $YNi_{2-x}(Co, Cu)_xB_2C$ solid solutions from experimental data using the following equation

$$\chi_P = N_A\mu_B^2 SN(E_F) = \qquad (3)$$
$$= 0.3233 \cdot 10^{-4} SN(E_F) \text{ (states per 1 eV per formula unit)},$$

where N_A is the Avogadro constant, μ_B is the Bohr magneton, and S is the Stoner parameter, is shown in Fig. 9.

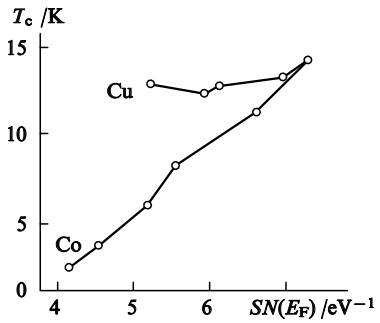


Figure 9. Correlation dependence of T_c on the reduced DOS at the Fermi level [$SN(E_F)$] for solid solutions $YNi_{2-x}(Co, Cu)_xB_2C$.

Thus, the reconstructed $T_c[SN(E_F)]$ dependences for Co and Cu impurities are substantially different. The only possible rationale for this fact can be relative strengthening of the electron–phonon interaction in alloys with the Cu → Ni type of substitution. The results of the investigation of the effect of the uniform compression on T_c for the systems in question [105] can be considered as indirect evidence in favour of the participation of both the electronic and electron-phonon mechanisms in the formation of superconducting properties of intermetallic borocarbides.

The effect of other impurities (Fe, Co, Ru, and Pd) on the superconducting properties of YNi_2B_2C has been considered by Bud'ko *et al.*[32] Linear suppression of the superconductivity effect with an increase in x was found in all cases. The data of Mössbauer spectroscopy and experiments on the magnetic susceptibility show that the dopants in the bulk of the initial phase have no local magnetic moments and their effect on the magnitude of the superconducting gap and thermodynamic properties is of local character.[106] Then T_c will be mostly affected by the $N(E_F)$ value, for which the change rate is proportional to the difference between the number of the valence electrons (z) of nickel and that of a substituting element.

Studies of the effects of sublattice doping on the electronic properties of IBC carried out by numerical quantum-chemical methods were started taking the $Y(Ni_{1-x}M_x)_2B_2C$ (M = Fe, Co, and Ru) solid solutions as an example.[73] Solid solutions with two different impurity concentrations ($x = 0.07$ and 0.47) approximated in the framework of the cluster approach by 71-atomic $Y_{12}(Ni,M)_{15}B_{32}C_{12}$ fragments with D_{2d} symmetry have been analysed.

The 'cluster' densities of the d states of Ni and substituting elements (Fe, Co, and Ru) in the $Y(Ni_{1-x}M_x)_2B_2C$ alloys for

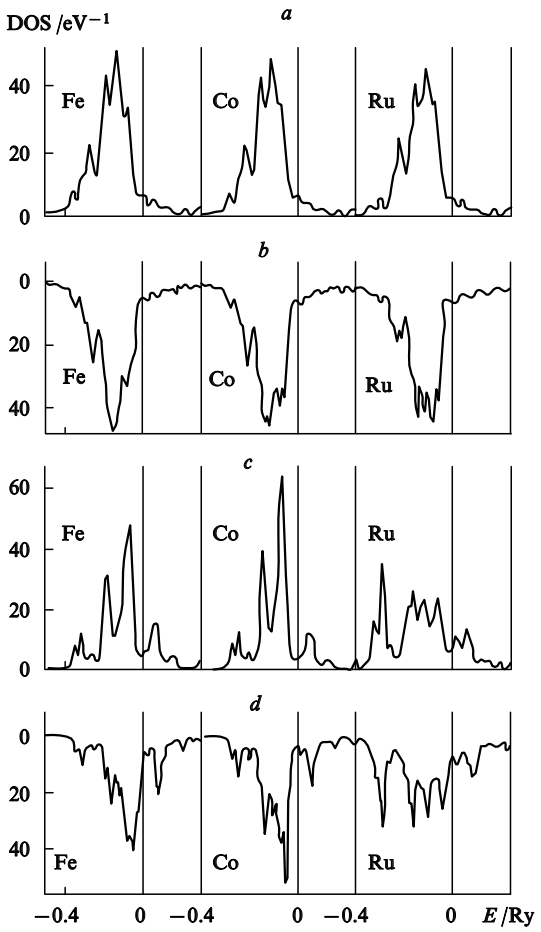


Figure 10. The 'cluster' densities of states for Ni (*a*, *b*) and substituting elements (M = Fe, Co, and Ru) (*c*, *d*) in $Y(Ni_{1-x}M_x)_2B_2C$ alloys for $x = 0.07$ (*a*, *c*) and 0.47 (*b*, *d*).

$x = 0.07$ and 0.47 are shown in Fig. 10 and the electronic configurations and atomic charges are listed in Table 7.

As should be expected from the rigid band model, doping the matrix with the *d* elements mentioned should decrease the E_F value and result in partial 'devastation' of the near-Fermi Ni3*d* states with the corresponding reduction of their populations. However, the populations of the Ni3*d* orbitals remain virtually unchanged, whereas the corresponding cluster LDOS become somewhat broadened. The local densities of states for Ni and dopants differ substantially. Thus, the high-energy region of the subband of *d* states for Fe and Co is vacant. In contrast to 3*d* impurities, the Ru4*d* states form a broad diffuse subband for all ruthenium concentrations. A low-energy peak (with an energy at the maximum of about −0.4 Ry) corresponding to localised Ru−B bonds in the NiB_4 tetrahedra and a three-peak structure of delocalised states can be seen on the LDOS profile. Additionally, one more LDOS peak appears at the Fermi level. A change in the effective charge of the Ni atoms occurs in the $Y(Ni_{1-x}M_x)_2B_2C$ alloys (Table 7); it is primarily due to breaking down the symmetry of the crystalline environment of these sites upon introduction of dopants and to the change in the population of the extended 4*s* and 4*p* orbitals of nickel.

It is of interest to follow the change in the extent of overlap of the wave functions for individual atoms (the covalent component of the bond) upon doping of YNi_2B_2C. The corresponding bond populations are listed in Table 8. The B−C interaction, which is the strongest in the original crystal, becomes weakened by ∼1%–4% upon introduction of impurities. The antibonding Y−C state remains almost unchanged, being localised in the plane nets. The N−B bond order is constant in the presence of Fe and Co; however, it decreases (by ∼3%) upon introduction of Ru. The overlap integrals for M−B bonds are larger than those for the Ni−B bond.

Table 7. Mulliken populations of valence orbitals and effective atomic charges in $Y(Ni_{1-x}M_x)_2B_2C$ substitution alloys.

Atom	Orbital population			q_{ef}
	d	*s*	*p*	
YNi_2B_2C				
Ni(1)[a]	0.06	0.38	0.52	+0.11
B	–	0.82	2.53	−0.35
Ni(2)[b]	2.11	0.41	0.39	+0.16
Y	0.54	0.06	0.05	+2.49
C	–	1.40	4.35	−1.75
$Y(Ni_{1-x}Co_x)_2B_2C$				
Co	8.23 / 8.24	0.33 / 0.33	0.46 / 0.49	+0.05 / 0.02
B	–	0.81 / 0.81	2.53 / 2.52	−0.34 / −0.33
Ni	9.10 / 9.10	0.41 / 0.42	0.39 / 0.38	+0.17 / 0.16
Y	0.54 / 0.54	0.06 / 0.06	0.05 / 0.05	+2.49 / +2.49
C	–	1.40 / 1.39	4.35 / 4.36	−1.75 / −1.75
$Y(Ni_{1-x}Fe_x)_2B_2C$				
Fe	7.28 / 7.35	0.31 / 0.30	0.45 / 0.41	+0.06 / −0.04
B	–	0.81 / 0.80	2.55 / 2.52	−0.36 / −0.32
Ni	9.10 / 9.11	0.41 / 0.42	0.39 / 0.38	+0.17 / +0.16
Y	0.54 / 0.54	0.06 / 0.06	0.05 / 0.05	+2.49 / +2.49
C	–	1.40 / 1.40	4.34 / 4.36	−1.74 / −1.76
$Y(Ni_{1-x}Ru_x)_2B_2C$				
Ru	7.48 / 7.50	0.25 / 0.24	0.43 / 0.38	+0.10 / 0.12
B	–	0.78 / 0.75	2.57 / 2.60	−0.36 / −0.34
Ni	9.10 / 9.07	0.41 / 0.43	0.40 / 0.43	+0.16 / +0.13
Y	0.55 / 0.56	0.07 / 0.07	0.05 / 0.06	+2.48 / +2.47
C	–	1.40 / 1.39	4.34 / 4.35	−1.74 / −1.74

Note. The values for the atoms of $Y(Ni_{1-x}M_x)_2B_2C$ alloys for $x = 0.07$ and 0.47 are given above and below the line, respectively. [a] The central nickel atom in the cluster. [b] Peripheral nickel atoms in the cluster.

The considered processes of rearrangement of the electron states in doped borocarbide alloys are illustrated by the contour plots of the difference charge density.[73] These contour plots show that both the covalent B−C bond and the charges on the yttrium atoms weakly 'respond' to the change in the composition of the M sublattice. The major effects of the electron density perturbation are localised near the substitution centre (in the bulk of the MB_4 tetrahedron). On the whole, the calculations [73] make it possible to interpret the chemical bonding in the $Y(Ni_{1-x}M_x)_2B_2C$ solid solutions as a combination of covalent-ionic-metallic interatomic

Table 8. Bond populations (e) in $Y(Ni_{1-x}M_x)_2B_2C$ solid solutions (M = Fe, Co, and Ru) according to discrete variational embedded-cluster calculations.

Composition, bond	YNi_2B_2C	$Y(Ni_{1-x}Fe_x)_2B_2C$		$Y(Ni_{1-x}Co_x)_2B_2C$		$Y(Ni_{1-x}Ru_x)_2B_2C$	
x	0	0.07	0.47	0.07	0.47	0.07	0.47
Ni – B	0.64	0.64	0.62	0.64	0.64	0.62	0.62
Y – C [a]	−0.18	−0.18	−0.18	−0.18	−0.18	−0.18	−0.18
B – C	1.14	1.12	1.13	1.13	1.13	1.09	1.12
M – C	0.66	0.72	0.72	0.68	0.69	0.68	0.67

[a] The negative value corresponds to antibonding of the Y – C bond.

interactions with a substantial spatial anisotropy, where the Y – C interaction in the plane nets and the interaction in M – B layers result from ionic and covalent binding, respectively, and the 'interlayer' (YC) – (MB) interactions are due to hybridisation of B and C atomic states. The doping of the M sublattice predominantly modifies the charge states and interspecies bondings in the M – B layers.

It is natural that the applicability of the cluster approach to the correct description of changes in subtle features of the TDOS (especially, near the Fermi surface, *viz*., in the region of strongly delocalised states), interpretation, and prognosis of superconducting and magnetic properties of multicomponent solid solutions is limited. Band calculations of borocarbide solid solutions of variable composition are needed.

VI. The energy band structure of 'two-layered' LnNiBC borocarbides and solid solutions based on them

In addition to the quaternary LuNiBC phase, a series of isostructural solid solutions of variable composition of the general formula $Ln(Ni_{1-x}M_x)BC$ (Ln = Lu, Y; M = Cu, V) have been synthesised to date.[36, 37, 42]

The energy band structure of LuNiBC was calculated by Mattheiss,[50] Kim,[68] and Coehoorn.[70] Let us discuss it in the framework of LAPW calculations.[50] The character of the $E(\boldsymbol{k})$ dependence for the near-Fermi bands is the most remarkable when comparing the valence band structures of $LuNi_2B_2C$ (Fig. 3) and LuNiBC (Fig. 11). The flat regions of the Ni3*d* bands ($G-X$), which virtually coincide with E_F for $LuNi_2B_2C$, appear to be shifted towards higher energies on the energy scale for LuNiBC. This results in the formation of the Ni3*d* resonance in the region of nonbonding states and the DOS at the Fermi level appears to be low ($N(E_F) \sim 1$ electron per cell). The E_F position in the region of the local DOS minimum in the electronic energy spectra of LuNiBC is reproduced in calculations performed by the ASW [70] and *ab initio* pseudopotential [68] methods.

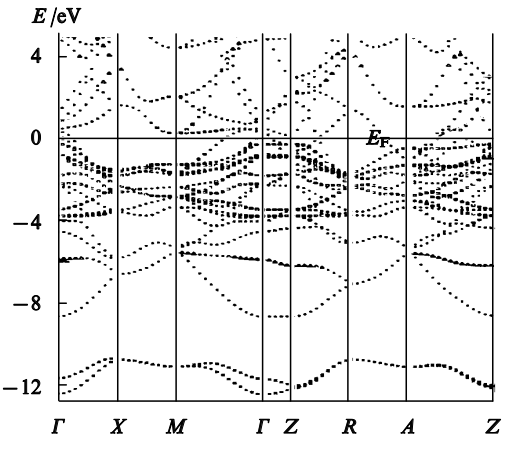


Figure 11. The band structure of LuNiBC.[50]

These peculiarities of the position of the Fermi level in the region of local DOS maximum ($LuNi_2B_2C$) and minimum (LuNiBC) are crucial for the explanation of distinctions between the superconducting properties of 'one-layered' and 'two-layered' IBC having similar crystalline structures and close interatomic distances. If the calculations [50, 58, 70] of electronic spectrum of LuNiBC are correct, one should expect that the $N(E_F)$ values of solid solutions will be increased as compared to that of an 'ideal' crystal (with the corresponding changes in properties) for any change in CVE (for instance, due to the doping of sublattices).

This assumption was tested by Qiu *et al*.[36, 42] and Gangopadhyay *et al*.[37] Thus, YBC, YB_4, and several other phases were present in the specimens of synthesised $LnNi_{1-x}Cu_xBC$ solid solutions (Ln = Y, Lu; $0 \leqslant x < 1$), the amount of tetragonal $YNi_{1-x}Cu_xBC$ phase decreased sharply with an increase in the copper concentration.[37] It was thus suggested that compounds YCuBC and LuCuBC are unstable.[37] The effect of dopant on the lattice constants of YNiBC (a = 3.579 Å, c = 7.570 Å) and LuNiBC (a = 3.495 Å, c = 7.663 Å) is worth noting. The value of parameter a increases most rapidly in the initial stage of doping (up to $x \simeq 0.2$), while a linear increase in the parameter c is observed at higher concentrations of copper. The rates of changes in the concentration (c) $\mathrm{d}\ln c/\mathrm{d}x$ for Y and Lu solid solutions are equal to 0.032 and 0.038, respectively, which is very close to that for $YNi_{2-x}Cu_xB_2C$ ($\mathrm{d}\ln c/\mathrm{d}x \simeq 0.03$).[42] This indicates a common nature of the observed effect, which can be related to the weakening of covalent M – B interactions upon partial Cu → Ni substitution due to the filling of the Ni3*d* orbitals by an additional electron of copper. The reason for considerable differences in the solubility limits of copper in 'one-layered' and 'two-layered' IBC, which amount to ~ 50% – 60% and 20%, respectively, remain unclear.

An increase in the content of copper results in the increase in T_c of $LnNi_{1-x}Cu_xBC$ solid solutions, the effect for yttrium compounds being more pronounced than that for lutetium compounds. The maximum T_c for YNiBC doped with copper is 8.9 K (at $x > 0.6$) is determined by tetragonal IBC and cannot be ascribed to impurities of other phases [YB_6 (T_c = 6.0 K), YB_{12} (T_c = 4.7 K), YC_2 (T_c = 3.8 K), YB_2C_2 (T_c = 3.0 K)] found in the specimens.[107] Gangopadhyay *et al*.[37] also pointed to the fact that T_c is dependent on the dispersity of the specimens; for instance, annealing of $YNi_{1-x}Cu_xBC$ specimens (for $x > 0.6$) considerably increases their T_c.

Extrapolation of the $T_c(x)$ dependence to $x = 1$, which corresponds to a hypothetical 'YCuBC', gives $T_c \simeq 10$ K, which is lower than for 'LuCuBC'. Presumably, the electronic structures of LuNiBC and YNiBC are similar and the $N(E_F)$ value for both compounds must increase upon introduction of copper atoms.

The inverse effect, namely, a decrease in CVE, upon partial substitution of nickel by vanadium in LuNiBC, was discussed by Qiu *et al*.[36] A series of single-phase $LuNi_{1-x}V_xBC$ solid solutions has been prepared and the solubility limit of vanadium is $x = 0.25$. The temperature dependence of electrical resistance has been measured and it has been found that T_c(LuNiBC) = 2.96 K and $T_c(LuNi_{0.8}V_{0.2}BC)$ = 2.60 K, *i.e*., $\mathrm{d}\ln T_c/\mathrm{d}x = -0.5$. Thus, E_F for the matrix does not coincide with the local DOS minimum and the $N(E)$ shape is more complex, since the Fermi level in LuNiBC can be intermediate in energy between the minimum and local

maximum of $N(E)$, hence, $dN(E)/dE > 0$. The study of the effect of external pressure on T_c shows that $dT_c/dP = -0.17 \pm 0.03$ K GPa^{-1} for both the original and doped IBC. From the viewpoint of the band theory, the effect of external pressure is equivalent either to broadening of the bands (at E_F = const) or to the E_F shift towards the lower-energy region. Hence, if E_F for LuNiBC coincides with the DOS minimum, then the $dN(E_F)/dP$ should be positive for both LuNiBC and $LuNi_{1-x}V_xBC$. The negative value of dT_c/dP can indicate either a more complex shape of the DOS distribution near E_F than was obtained from the one-electron band calculations or the impossibility to describe the effect of hydrostatic pressure on T_c by a simple correlation with the change in $N(E_F)$.

VII. Electronic structure and some physicochemical properties of intermetallic borocarbides

The nature of IBC is determined by (or is closely related to) their electronic structure and can be rationalised from the viewpoint of theoretical models of EES for intermetallic borocarbides.

1. Superconductivity

The superconductivity of IBC is the property that attracted attention to this class of compounds and gave rise to numerous experimental and theoretical studies. The first calculations of EES of $LuNi_2B_2C$, LuNiBC, and YNi_2B_2C (see Refs 50, 59, 64, 70, and 71) made it possible to place the IBC with certainty into the class of conventional superconductors with the BCS type of conductivity, to determine specific features of the structure of the near-Fermi energy bands for one- and two-layered IBC, and to relate their conducting properties to specific electron states on the Fermi surface. These concepts are widely used for qualitative interpretation of the results obtained. As has been noted above, the attempts were made to extend them (using the rigid band model) to multicomponent solid solutions. It was assumed, in the simplest case, that $T_c \sim N(E_F)$, which, in turn, is determined by the degree of filling the valence band depending on CVE for the compound of a given composition.

An attempt to find correlations between the parameters of the one-electron energy spectra of solid solutions $Y(Ni_{1-x}M_x)_2B_2C$ (M = Fe, Co, and Ru) (these parameters were obtained in the framework of the cluster approach) and T_c has been undertaken by Zeng *et al.*[73] The integrated density of the *d* states of transition-metal atoms (N_d) in solid solutions of variable composition, which is used in the theory of paired electron correlations and associated with the conditions for the formation of superconducting state, was considered as the 'electronic factor' of superconductivity. The N_d value can be calculated using the following formula

$$N_d = \int_{-\infty}^{E_F} D_d^q(\varepsilon) d\varepsilon \,, \tag{4}$$

where $D_d^q(\varepsilon)$ is the sum of partial populations of the *d* states of the *q*-type atoms

$$D_d^q(\varepsilon) = \sum_i P_{d,i}^q \frac{\delta\pi}{(\varepsilon - \varepsilon_i)^2 + \delta^2} \,. \tag{5}$$

Here, $P_{d,i}^q$ is the Mulliken population of the atomic orbital *d* in the cluster orbital ϕ_i with the energy eigenvalue ε_i, δ is the half-width ($\delta = 0.136$ eV) of the Lorentzian function employed to simulate the energy broadening of the discrete cluster levels in the crystal, and summation is performed over all occupied orbitals *i*.

In the rigid band model, the integrated density of *d* states for a binary alloy of variable composition $A_{1-x}B_x$ can be written as

$$N_d^{AB} = (1-x)N_d^A + xN_d^B \,,$$

where N_d^A and N_d^B are populations of the *d* states for 'pure' metals A and B. Thus, the corresponding populations for the $Ni_{1-x}Fe_x$ alloy are usually assumed to be ~ 9 e$^-$ (Ni) and ~ 7 e$^-$ (Fe). This primitive scheme for the solid solutions under consideration (for instance, $Y(Ni_{1-x}Fe_x)_2B_2C$) can be refined using formula (6)

$$\overline{N_d} = 9(1-x) + 7x + N_d^0 \,, \tag{6}$$

where N_d^0 describes the effects of hybridisation of the transition metal (Ni), that is substituted, with the nearest environment ($Ni-B_4$).

Comparison of N_d values obtained from self-consistent calculations on selected clusters and the values of $\overline{N_d}$ parameters of a given model found from Eq (6) ‡ allows one to test the rigid band model.

Calculations performed by Zeng *et al.*[73] showed that the N_d and $\overline{N_d}$ values are fairly close for low impurity concentrations ($x = 0.07$) and the T_c *vs.* N_d correlation dependence is clearly observed. The difference between the parameter of the model $\overline{N_d}$ and the self-consistent N_d value increases substantially as the M content increases.

Direct estimates of T_c based on the results of calculations of the energy band structure of IBC were made by Mattheiss *et al.*,[50,64] Pickett *et al.*,[59] Kim *et al.*,[68] and Ravindran *et al.*[72] The constant of the electron–phonon interaction (λ) was found to be approximately equal to 2.6 and the frequency of the Ba_{1g} phonon mode for $LuNi_2B_2C$ is 850 cm^{-1}.[59] It is assumed that the soft modes of heavier atoms also make contributions to the superconductivity. Taking into account a mixed character of highest filled bands, it is emphasised that the multicomponent nature of the phase is one of the main factors that determine the superconductivity of IBC.

The electron–phonon mechanism of superconductivity in $LuNi_2B_2C$ owing to the interaction between an isolated *sp* band near the Fermi level and high-frequency Ba_{1g} phonons modulating the angles of NiB_4 tetrahedra was discussed by Mattheiss *et al.*[64]

The T_c value ($\simeq$15 K) found for YNi_2B_2C using $\lambda = 0.9$, the experimental Debye temperature ($\Theta = 573$ K),[74] and the calculated $N(E_F)$ value is in good agreement with the experiment.[71]

Kim *et al.*[68] estimated the λ value from the data on measurements of low-temperature electronic heat capacity γ (see Ref. 56) and band calculations using the McMillan formula [4] and found that $\lambda \simeq 0.8-1.1$. The relatively high T_c value for $LuNi_2B_2C$ is primarily determined by considerable contributions of the Ni3*d* states to $N(E_F)$ [68] and the assumed mechanism of the interaction between the high-frequency a_{1g} mode and *sp* nonmetal bands [64] cannot play the decisive role, since the contributions of the boron and carbon atomic states to $N(E_F)$ are small. Then, an estimate of the T_c value for the related borocarbide LuNiBC using a rough approximation $T_c \simeq N(E_F)$ can be made and the results obtained ($T_c \sim 0.7-2.6$ K) are close to the experimental data.

Despite the above disagreement on the relative role of the electron and vibrational states of individual atoms and atomic groups in the formation of superconducting properties of IBC, all calculations [50,59,64,68,71] allow one to consider these compounds as the 3*D* systems with an intermediate type of the electron–phonon interaction and superconductivity described by the BCS theory.

In this connection the studies of the isotope effect [108] and some electronic properties of IBC [109] should be mentioned. They suggest rather strong electron–phonon interactions in these systems. The phonon anomalies similar to those found in superconducting 3*D* carbides were found in borocarbides.[110] An additional phonon mode associated with the formation of superconducting state was reported by Kawano *et al.*[111]

A progressive suppression of the real part of optical conductivity $\sigma_1(\omega)$ in the far IR region, as should be expected in accord with the BCS theory in the case of appearance of a superconducting gap (Δ), was observed for YNi_2B_2C and $LuNi_2B_2C$ in the

‡ In this case, the N_d^0 value for the original matrix ($x = 0$) is obtained from the condition $N_d = \overline{N_d}$.

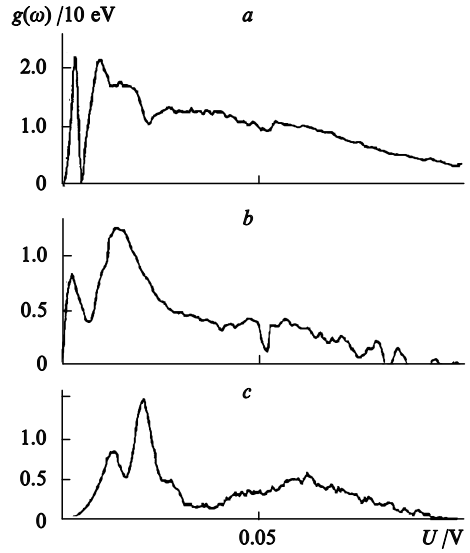


Figure 12. The PCS function of the electron–phonon interaction for $HoNi_2B_2C$ (*a*), YNi_2B_2C (*b*), and $LaNi_2B_2C$ (*c*).[114]

studies of the temperature dependence of $\sigma_1(\omega)$ at $T < T_c$.[112] At $T \simeq 6$ K and frequencies 5.6 meV ($LuNi_2B_2C$) and 6.9 meV (YNi_2B_2C), the $\sigma_1(\omega)$ values are equal to zero. This makes it possible to estimate the $2\Delta/k_BT_c$ value as $\sim 3.9-5.2$. Hence, the effect of the formation of the Cooper pairs is assumed to occur with participation of the low-frequency phonon modes (optical phonons).[113]

The electron–phonon interaction in a number of IBC was studied by the point contact spectroscopy (PCS),[115] which makes it possible to observe directly the interactions of the conduction electrons with elementary excitations in the crystal.

The PCS functions $g(\omega)$ for $HoNi_2B_2C$, YNi_2B_2C, and $LaNi_2B_2C$ are shown in Fig. 12. It can be seen that the function $g(\omega)$ for $HoNi_2B_2C$ has two distinct maxima with energies corresponding to the DOS peaks of soft phonons. A similar structure of the function $g(\omega)$ is observed for YNi_2B_2C, which indicates an electron-phonon interaction with low-energy phonons ($h\nu \simeq 4-9$ meV). On the contrary, the corresponding interaction was not observed for nonsuperconducting $LaNi_2B_2C$ in the soft mode region of the phonon spectrum. Bommeli *et al.*[112] explain the above distinctions by specific features of the electronic structure (in particular, by the nesting effect on the Fermi surface) of the considered representatives of IBC homologous series.

2. Superconductivity and magnetism

The relationship between superconductivity and magnetism is one of the central problems of modern physical chemistry of crystals. For ternary intermetallic borides, this problem has been discussed in detail in a monograph.[116] It has been noted in early studies of the properties of IBC that most LnM_2B_2C phases are magnetic superconductors;[1–3,19] therefore, the problems of coexistence and mutual influence of magnetism and superconductivity were considered first in numerous experimental studies.

The results obtained to date make it possible to state that IBC are a unique class of magnetic superconducting materials. It is known that the onset of a magnetic order leads to an abrupt suppression of superconductivity and in the case of coexistence of both effects they are observed at appreciably different temperatures (energies). In this case, the temperature of magnetic ordering (the Neel temperature, T_N) is, as a rule, much lower than T_c for all the known groups of magnetic superconductors. Thus, T_c in Chevreul's phases is higher than T_N (~ 1 K) by an order of magnitude.[116] The differences between T_c and T_N for HTSC cuprates containing rare-earth metal ions are even larger.[107]

On the contrary, in the case of IBC the magnetic and superconducting states exist in the same temperature range and T_c can be either higher or lower than T_N.

T, K	$ErNi_2B_2C$	$GdNi_2B_2C$	$DyNi_2B_2C$
T_N	6.8	19.0	10.6
T_c	11.0	2.0	6.0

If T_N and T_c values are comparable, then the energy effects of the magnetic ordering and electron-electron interaction through the lattice phonons (formation of the Cooper pairs), *i.e.*, the energies of formation of magnetic structures and the energies of superconducting states, will also be close. Such a unique feature caused an ever increasing number of publications devoted to the investigation of relationship between the magnetism and superconductivity of IBC.

The greatest progress in this line has been achieved in the studies of magnetic structures of IBC. The investigations were mostly carried out by X-ray or neutron diffraction techniques for $PrNi_2B_2C$ and $DyNi_2B_2C$,[14,19,20,23,100,117–132] $ErNi_2B_2C$ and $TbNi_2B_2C$,[21,22,47,133–135] $TmNi_2B_2C$,[11,47,136–138] $GdNi_2B_2C$,[25,45–47] and $CeNi_2B_2C$ and YNi_2B_2C.[47,139]

As a result, a wide variety of magnetic IBC structures was found; some of them are listed in Table 9. Thus, an antiferromagnetic ordering was found for $LnNi_2B_2C$ (Ln = Pr, Dy, and Ho) at low temperatures. The antiferromagnetic structure is formed due to alternation of antiferromagnetically oriented rare-earth metal layers with ferromagnetic type of intralayer ordering of magnetic moments along the *z* axis. The magnetic structure of $ErNi_2B_2C$ can be described by the spin density waves (SDW) with the wave vectors $\boldsymbol{q}(001)$ or $\boldsymbol{q}(110)$. Several magnetic structures were found for $HoNi_2B_2C$ ($T_c \simeq 8$ K). At $T_N \simeq 8.5$ K, a helical incommensurate antiferromagnetic structure appears, in which the plane nets of vectors of ferromagnetically oriented moments of are rotated by an angle of $\sim 17^\circ$ with respect to the original antiparallel packing. The wave vector of this incommensurate spin structure is $\boldsymbol{q}(0, 0, 0.91)$. Another type of incommensurate structure modulated along the *x* axis by the wave vector $\boldsymbol{q}(0.55, 0, 0)$ exists at $T_N \simeq 6.5$ K (in the region of the reentrant superconducting transition with $T_c \simeq 5$ K). The helical structure is destroyed with the formation of a conventional antiferromagnetic order as the temperature decreases. It is important that the magnetic structures are extremely sensitive to the IBC composition.[140,141]

Currently, there is no general microscopic theory of superconductors having incommensurate magnetic structures. Only assumptions on the nature of coexistence and relationship between the superconductivity and magnetism have been made.[10,14,23,47,117–139]

Table 9. Types of magnetic structures, magnetic moments (μ), the Neel temperatures (T_N/K) critical temperatures (T_c/K), and magnetic wave vectors ($\boldsymbol{q}$) for several IBC.[47]

Phase	Type of magnetic structure	T_N	T_c	μ, μ_B	$\boldsymbol{q}$
$PrNi_2B_2C$	AF	4.0	–	0.81	(0, 0, 1)
$NdNi_2B_2C$	AF	4.8	–	2.10	(1/2, 0, 1/2)
$GdNi_2B_2C$	ISS(*x*)	19.0	–	7.0	(0.55, 0, 0)
$TbNi_2B_2C$	ISS(*y*)	15.0	–	7.78	(0.555, 0, 0)
$DyNi_2B_2C$	AF	10.6	6	8.47	(0, 0, 1)
$HoNi_2B_2C$	ISS(*z*)	8.5	8	6.7	(0, 0, 0.91)
	ISS(*x*)	6.3	–	–	(0.55, 0, 0)
	AF	5.0	5	8.62	(0, 0, 1)
$ErNi_2B_2C$	SDW(*x*)	6.8	11	7.19	(0.553, 0, 0)
$TmNi_2B_2C$	SDW(*z*)	1.5	11	3.78	(0.093, 0.093, 0)

Note. The following designations are used: AF is antiferromagnetic structure, ISS(*x*, *y*, *z*) is incommensurate spin structure with the wave vector modulated along the (*x*, *y*, *z*) directions, and SDW(*x*, *y*, *z*) is spin density waves along the (*x*, *y*, *z*) directions.

Thus it has been shown in one of the first studies of LnM_2B_2C (Ln = Tm, Er, Ho, and Dy) [10] that their properties are similar to those of magnetic superconductors $LnRh_4B_4$ and $LnMo_6S_6$.[142, 143] In the latter compounds, the high density of local magnetic moments (the long-range spin order) and superconductivity 'coexist' owing to the spatial separation of magnetic rare-earth metal ions and transition-metal ions, a weak exchange interaction between the states of these sites, and a low density of the conduction electrons at the sites occupied by the 4*f* elements.

The vast majority of theoretical investigations of EES are devoted to IBC containing nonmagnetic rare-earth metal atoms (Y and Lu) and carried out for a spin-restricted (nonmagnetic) version. Quantitative calculations of the electron states taking into account the spin order were performed only for $GdNi_2B_2C$ assuming the ferromagnetic ordering of magnetic moments.[70] The first attempt to explain the magnetic order from the viewpoint of one-electron band structure calculations of IBC has been undertaken by Grenwood *et al.*[144] The ordering of magnetic moments was assumed to occur due to an indirect interaction (of the Ruderman – Kittel – Kasuga – Yoshida type) of 4*f* electrons of the rare-earth metal atoms. Then, the onset of magnetic order can be correlated with the maxima of magnetic susceptibility $\chi(\boldsymbol{q})$ of the conduction electrons, which, in turn, are determined by the distribution of states on the Fermi surface (in particular, by the nesting effect). The calculations [144] showed that the $\chi(\boldsymbol{q})$ peaks appear near the wave vectors $\boldsymbol{q}$ = (0.6, 0, 0) and (0, 0, 0.9) along the $\boldsymbol{a}^*$ axis and near the wave vectors $\boldsymbol{q}$ = (0, 0, 0.3) and (0, 0, 0.9) along the $\boldsymbol{c}^*$ axis. These wave vectors correspond to the observed incommensurate SDW for $HoNi_2B_2C$.[19]

It should be noted again that most of the problems of the fundamental theory of superconducting magnetic IBC remain unexplored to date. They include, in particular, the problems of the onset of the magnetic order in superconducting materials, conditions of compatibility of and competition between these phenomena, the nature of the exchange interaction between magnetic ions and the conduction electrons, the role of the spin-orbital interaction, *etc*.

3. The electric field gradient

The electric field gradient (EFG) reflects the asphericity of the charge density distribution near the nucleus in question and is directly related to the electron density distribution in the crystal, the nature of the chemical bond, and the symmetry of the nearest environment of the nuclei. It is possible to determine the EFG value by studying the quadrupole effects in NMR spectra [145] and the Mössbauer effect.[146] Experimental estimates of EFG for compounds in question were performed for the ^{155}Gd nuclei in $GdNi_2B_2C$ and $GdCo_2B_2C$ (see Ref. 70) and ^{57}Fe for $Y(Ni_{1-x}Fe_x)_2B_2C$ alloys.[73]

The electric field gradient at the ^{155}Gd nuclei reflects first of all the asphericity of the 6*p* electron density distribution within a radius of ~ 2 Å.[147] The positive contributions to the V_{zz} EFG obtained for $GdNi_2B_2C$ and $GdCo_2B_2C$ points to considerable contribution of the $6p_x$,p_y orbitals localised in the plane of Gd – C nets to the charge density.

A quantitative EFG analysis was carried out using ASW calculations of the low-temperature $GdNi_2B_2C$ phase under the assumption of ferromagnetic spin order.[70, 148] The values of local magnetic moments at the Gd, Ni, B, and C atoms were 7.27, 0.03, 0.00, and -0.01 μ_B, respectively. The contributions of the populations (n_i) of the Gd 6*p* and 5*d* orbitals to the EFG and the radial charge densities $\langle r^{-3}\rangle_i$ were calculated using the following equations [148]

$$V_{zz}(6p) = 7.74\left[\frac{1}{2}(n_x + n_y) - n_z\right]\langle r^{-3}\rangle_{6p}\,, \tag{7}$$

$$V_{zz}(5d) = 5.54\left[\frac{1}{2}(n_{x^2-y^2} + n_{xy}) - \frac{1}{2}(n_{xx} + n_{yz} - n_{3z^2-r^2}\right]\langle r^{-3}\rangle_{5d}\,.$$

Table 10. Orbital populations (n_i), radial charge densities ($\langle r^{-3}\rangle_i$), and EFG components (V_{zz}) at ^{155}Gd nuclei for ferromagnetic $GdNi_2B_2C$ according to the ASW calculations.

Parameter	Spin 'up'	Spin 'down'
$n_x = n_y$ /e	0.173	0.165
n_z /e	0.147	0.132
$n_{z^2-y^2}$ /e	0.216	0.148
n_{xy} /e	0.304	0.278
$n_{xz} = n_{yz}$ /e	0.235	0.178
$n_{3z^2-r^2}$ /e	0.285	0.227
$\langle r^{-3}\rangle_{6p}$ /e a_0^{-3}	25.9	29.0
$\langle r^{-3}\rangle_{5d}$ /e a_0^{-3}	1.83	1.44
10^{21} $V_{zz}(6p)$ /V m^{-2}	5.21	7.41
10^{21} $V_{zz}(5d)$ /V m^{-2}	0.0	0.16

The values obtained are listed in Table 10. It can be seen that the $\langle r^{-3}\rangle_{6p}$ values are much larger than $\langle r^{-3}\rangle_{5d}$, *i.e.*, that the V_{zz} values are determined mainly by the asphericity of the 6*p* charge density. The calculated V_{zz} value (12.8×10^{21} V m^{-2}) virtually coincides with the experimental one (11.9×10^{21} V m^{-2}) obtained from the analysis of the Mössbauer spectra.[148]

Mulder *et al.*[148] emphasise that the V_{zz} value for $GdNi_2B_2C$ is comparable to the EFG value for the known magnetic materials $Ln_2Fe_{14}B$, $Sm_2Fe_{17}N_3$, and $LnCo_5$ (see Refs 149 – 151) and is remarkable in connection with the macroscopic magnetic anisotropy of IBC. However, the V_{zz} contribution of isostructural BCT phases ($GdNi_2Si_2C$, $GdCo_2Si_2C$) is small and negative.[147] It is suggested [148] that carbon atoms filling the vacancies of $ThCr_2Si_2$-like sublattice play the key role in the formation of IBC. The role of the carbon atoms is thought to be analogous to that of the nitrogen atoms, whose insertion into the bulk of intermetallic Sm_2Fe_{17} results in redistribution of the electron density around the samarium nucleus in such a way that the EFG in the formed nitride $Sm_2Fe_{17}N_3$ increases by $\sim 100\%$.[152]

The EFG values at the nuclei of transition-metal atoms in alloys of composition $Y(Ni_{1-x}M_x)_2B_2C$ (M = Fe, Co, and Ru; x = 0.07 and 0.47) were calculated in the framework of the cluster approach;[73] the following individual components responsible for the formation of the EFG tensor at the nuclei were estimated: V_{zz}^{val}, *i.e.*, the EFG dependent on the asymmetric distribution of valence electrons of the atom under consideration,

$$V_{zz}^{val} = \left\langle \frac{\rho(3z^2 - r^2)}{r^5} \right\rangle, \tag{8}$$

and V_{zz}^{nucl}, which includes the contribution of point charges Q_v and polarisation of inner shells

$$V_{zz}^{nucl} = \sum_v \frac{Q_v(3z_v^2 - r_v^2)}{r_v^5}, \tag{9}$$

where the summation is performed over the atoms of the calculated fragment.

Generally, one should also take into account the contribution of V_{zz}^{host}, which describes the effect of the crystal 'residue' ('external' with respect to the cluster selected) and whose nature is similar to that of V_{zz}^{nucl}. In several studies (see, for instance, Ref. 70), the V_{zz}^{host} value is assumed to be negligible by analogy with the results of calculations of ionic compounds.[153] The V_{zz}^{val}, V_{zz}^{nucl}, and V_{zz} values are listed in Table 11.

The EFG for transition metals is known to be determined by the asphericity of the distribution of *d* and *p* electrons.[154] The positive V_{zz}^{val} values (see Table 11) show that the contributions of $d_{x^2-y^2}$, d_{xy}, p_x, and p_y orbitals of transition metals (in the *xy* plane) dominate over those of d_{z^2}, d_{xz}, d_{yz}, and p_z orbitals oriented along the *z* axis. The small concentration differences in V_{zz}^{val} indicating the local nature of the EFG formation also worth noting. Estimates of the quadrupole splitting value proportional to the

Table 11. The EFG components (e a_0^-) at the transition-metal nuclei in $Y(Ni_{1-x}M_x)_2B_2C$ (M = Fe, Co, and Ru) alloys according to discrete variational calculations.

Central atom in the cluster	x	V_{zz}^{val}	V_{zz}^{nucl}	V_{zz}	$10^{17}\,V_{zz}$ /V cm^{-2}
Ni	0.00	0.74	−0.65	0.09	0.87
Fe	0.07	0.61	−0.65	−0.04	−0.39
Fe	0.47	0.50	−0.63	−0.13	−1.26
Co	0.07	0.27	−0.65	−0.37	−3.59
Co	0.47	0.24	−0.64	−0.40	−3.89
Ru	0.07	1.96	−0.65	1.31	12.7
Ru	0.47	1.95	−0.63	1.32	12.8

EFG value for iron in $Y(Ni_{1-x}Fe_x)_2B_2C$ alloys appeared to be in reasonable agreement with those obtained by Mössbauer spectroscopy.[33]

4. Atomic properties

Physicochemical characteristics of the solids determined by the total energy of their electron–nuclear system (E_{tot}) or by their cohesion energy (E_{coh}) are usually considered as their atomic properties. Direct calculations of E_{tot} and E_{coh} using modern quantum-chemical methods make it possible to determine many of the properties of crystals, namely, the equilibrium volumes and lattice parameters, bulk moduli, critical pressures (breaking stress of a chemical bond), and a number of thermodynamic parameters.[155, 156]

To date, these parameters have been calculated only for YNi_2B_2C in the framework of the LMTO approach.[69] Thus, calculation of the contributions of the atoms of different types (the so-called structural energies ΔE)[72] makes it possible to understand, in particular, the role of individual elements in the formation of the crystal structure of IBC. It has been found that ΔE values for Y and Ni are negative, whereas they are positive for the metalloid atoms (with respect to E_{tot} of neutral atoms), which implies that metallic components play the key role in the phase formation of IBC. Despite the destabilising (positive) energy of carbon, its incorporation into the structure results in an appreciable increase in the bonding energy of yttrium, *i.e.*, in the overall stabilisation of the phase. This is confirmed by calculations of the heat of formation of YNi_2B_2C: $\Delta H = -153.82$ Ry per formula unit.

Ravindran *et al.*[72] reported the solution of the equation of state for YNi_2B_2C (which makes possible studying the $P-V$ dependences[157, 158]) as a universal relationship between the volume of the crystal and its total energy. Theoretical values of the bulk modulus ($B_0 = 1.071$ kbar) and its first derivative have been obtained. Their comparison with the corresponding values for YRh_3B indicates a greater plasticity of YNi_2B_2C, which is likely associated with its layered structure.[72] Unfortunately, thermomechanical characteristics of IBC have not virtually been studied.

In our opinion, systematic calculations of the atomic characteristics of IBC of different composition and structure must be an effective method of attacking the problems of thermobarochemistry and theoretical material science of IBC and related compounds.

VIII. Spectroscopic studies of the electronic structure of intermetallic borocarbides

Spectroscopic methods make it possible directly to investigate the distribution of partial and total densities of filled and free states in a wide energy interval using X-ray emission, X-ray absorption, and X-ray photoelectron spectra (XES, XAS, and XPES, respectively). It is natural that the first band structure calculations were followed by spectroscopic studies of IBC. The main problems of such studies were testing the correctness of suggested theoretical models and determining specific features of the distribution of the electron states in excited electronic subsystems.

1. X-Ray photoelectron spectra

The XPES method was first used in studies of the distribution of the YNi_2B_2C electron states (Fig. 13).[159, 160] As can be seen, the XPES contains a peak of maximum intensity (~ 1.4 eV lower than the Fermi level) corresponding to the distribution of the Ni3*d* states, and local maxima with energies (E) 4.6, 6.2, 9.2, and 13 eV corresponding to *s* and *p* energy bands of boron and carbon.. The doublet structure of the Y4*p* core level is detected at $E \simeq 25$ eV. The edge structure of the near-Fermi photoelectron emission matched to the YNi_2B_2C DOS obtained from LAPW calculations[50, 59] and corrected for the effective cross-sections of photoionization of the individual states[161] is shown in the inset. The calculations reproduce the spectral structure sufficiently well. The narrowing of the width of the experimental peak (of the Ni3*d* type) and the shift of its maximum (by ~ 0.25 eV) towards lower bonding energies are the most pronounced differences between the calculated and experimental spectra. In addition, the DOS peak with an energy equal to E_F, predicted by quantum-chemical calculations, is not detected in the experiment.

The discrepancies between the results of calculations of the nonexcited states of YNi_2B_2C and its XPES can be explained using the resonance emission experiments.[159] The XPES were studied in the range of photon energies $h\nu = 64-74$ eV, *i.e.*, near the excitation threshold of Ni3*p* core levels. In this case, a satellite peak with energy $E \simeq 8$ eV is clearly seen on the high-energy side of the main spectral maximum.

This phenomenon, which is known for many metals, alloys, and compounds as resonance photoemission,[162–166] is accounted for by excitation of the Ni 3*p* core level and interference of direct processes of excitation of 3*d* photoelectrons and the processes involving super-Kronig–Coster transitions $3p^53d^{10}4s \rightarrow 3p^63d^84s + \varepsilon l$, where εl is a free electron.

Thus, the experimentally measured width of the 3*d* band for metallic nickel is by about 30% smaller than that obtained from LEDF calculations of the ground state, and a satellite is observed in the spectrum (~ 6 eV lower than E_F) due to the effects of electron correlation in the *d* band.[162, 163] The reason for the appearance of the satellite for NiO (~ 10 eV lower than E_F)[165] is analogous. Thus, the indicated discrepancies between the calculations and XPES of YNi_2B_2C can be associated with the redistribution of the 'spectral' density between the energy interval of localisation of the band of nonexcited states and lower-energy region (the appearance of the satellite due to the effect of electron correlation).

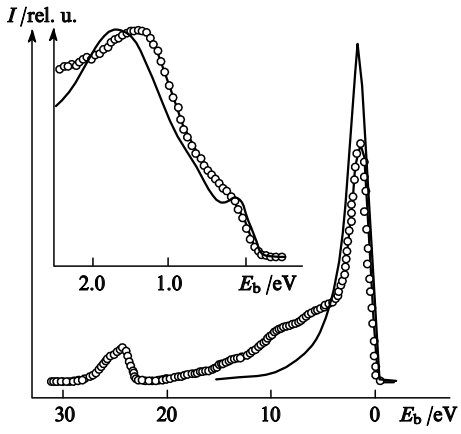


Figure 13. X-Ray photoelectron spectra of YNi_2B_2C ($h\nu = 60$ eV). The high-energy near-edge structure of photoemission ($h\nu = 20$ eV) is shown in the inset. Solid lines correspond to the theoretical XPES spectra obtained from the band LAPW calculations.

Peculiarities of the distribution of free states near the Fermi level in YNi_2B_2C were studied [160] by the inverse XPES method also known as X-ray bremsstrahlung (isochromat) spectroscopy (XBIS). The XBIS spectrum obtained [160] corresponds mainly to the Ni3*d* conduction band shifted by $\sim$ 1.5 eV with respect to E_F and to a partially unfilled Y4*d* band with its centre $\sim$ 6 eV above the E_F. For both XPES and XBIS, the suppression of spectral intensity near E_F is observed. This can be connected with narrowing of the near-Fermi conduction bands due to the interaction with low-energy excitations (the appearance of a pseudogap as a result of electron–phonon interactions,[167,168] the interaction of electrons with spin fluctuations [169]).

The main reason for discrepancies between the results obtained by the XPES method and the band theory, namely, redistribution of 'spectral' density towards higher bonding energies near E_F for YNi_2B_2C and $LuNi_2B_2C$, is discussed by Fujimori *et al.*[170] It has been suggested to explain the transfer of the 'spectral' density from the near-Fermi region of coherent quasiparticle excitations to the region of incoherent excitations (more distant from the E_F) by renormalisation of the mass of the conduction band; the macroscopic description of this effect should take into account the electron-electron interactions.

2. X-Ray emission spectra

The XES studies of the partial DOS distribution were carried out for YNi_2B_2C and LuNiBC (see Ref. 171) and for YNi_2B_2C and $LaNi_2B_2C$ (see Ref. 172).

The BK_α and CK_α emission spectra of YNi_2B_2C and LuNiBC and the LDOS of B and C atoms calculated by Mattheiss [50] are presented in Fig 14. As can be seen, the positions of the main spectral peaks are in agreement with the distribution of the B2*p* and C2*p* states. The contributions from low-energy bands (mainly of the 2*p* type) of nonmetals are not detected in K_α XES, since they are forbidden by the dipole selection rules; the spectra exhibit the presence of a density of boron and carbon 2*p* states near E_F for YNi_2B_2C, and their presence in this region is associated with the effect of B2*p*–Ni3*d*–C2*p* hybridisation.[171]

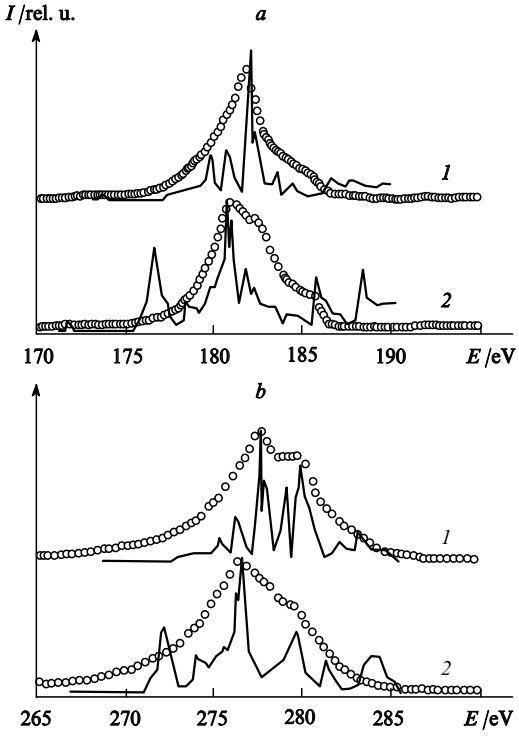


Figure 14. The BK_α (*a*) and CK_α (*b*) X-ray emission spectra of LuNiBC (*1*) and YNi_2B_2C (*2*). Solid lines correspond to local DOS of the B and C 2*s* and 2*p* AOs according to the LAPW calculations.[50]

Fluorescence (B, C)K_α XES of polycrystalline specimens of YNi_2B_2C and $LaNi_2B_2C$ have been analysed by Shin *et al.*[172] After comparing the parameters of the BK_α and CK_α spectra of both IBC, the authors have noted that the BK_α lines appeared to be more sensitive to structural distortions on going from YNi_2B_2C and $LaNi_2B_2C$, which implies that the metal–nonmetal hybridisation occurs mainly due to the B2*p* states. Comparison of intensities of the BK_α XES of IBC near E_F shows that this value for the superconducting YNi_2B_2C is $\sim$ 10% larger than that for $LaNi_2B_2C$ and, hence, B2*p* states play an important role in the formation of superconducting properties of IBC.

3. X-Ray absorption spectra

Pellegrin *et al.*[173] studied the structure of the bottom edge of the conduction band of polycrystalline $LnNi_2B_2C$ (Ln = Y, Sm, Tb, Ho, Er, Tm, Lu) specimens by B$K(1s \rightarrow 2p)$ and Ni$L_{2,3}(2p_{2/3} \rightarrow 3d, 4s)$ XAS. It has been found that the shape of the Ni*L* spectra is nearly the same for all IBC studied, *i.e.*, that the degree of filling of Ni3*d* and 4*s* bands is independent of the nature of the Ln atoms. Hence, the observed differences in T_c for these phases are not related to the position of E_F with respect to the centre of the Ni3*d* band, but are determined by the effect of the magnetic unpairing of the Cooper pairs. The lines of the Ni*L* XAS of IBC were found to be shifted (by $\sim$ 1 eV) toward the high-energy region relative to metallic nickel, which is accounted for by the chemical shift of the Ni2*p* level in borocarbides due to a partial Ni $\rightarrow$ B, C charge transfer, which also involves the density of Ni4*s* electrons.

For B*K* XAS, on the contrary, pronounced distinctions depending on the lanthanide type were observed between spectral lines in the region 4–7 eV above E_F, which might be due to the lanthanide effect on the degree of distortion of the NIB_4 tetrahedra.

Matching the B*K* and Ni$L_{2,3}$ absorption spectra using a unified scale (Fig. 15) indicates an appreciable covalent overlap of Ni–B outer states. Thus the four clearly seen extrema of the Ni$L_{2,3}$ spectrum (see Fig. 15, points *b*, *c*, *d*, and *e*) have their isoenergetic analogues in the structure of the B*K* spectrum and reflect a rather strong Ni3*d*–B2*p* interaction. The peak of the B*K* spectrum corresponds to the C2*p*–B2*p* covalent interaction.

Comparison of the absorption spectra and partial densities of unfilled states indicates [173] that the one-electron methods of the band theory reproduce the electronic energy distributions in this spectral region fairly well. An appreciable broadening of XAS spectral bands as compared to the results of calculations can be due to the electron–photon interaction.

The XAS method was also used for the determination of cerium valence in $CeNi_2B_2C$ and solid solutions $Y_{1-x}Ce_xNi_2B_2C$.[174] As has been mentioned above, in its crystallographic

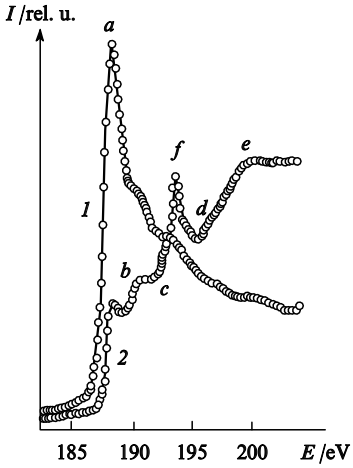


Figure 15. The near-edge structure of the B*K* (*1*) and Ni*L* (*2*) absorption spectra of $ErNi_2B_2C$.

characteristics $CeNi_2B_2C$ is an exception to the morphological series of IBC, namely, its lattice constant a is larger, whereas the lattice constant c is smaller than those expected from the lanthanide compression rule. Presumably, the above anomaly is associated with the variable valence of Ce; an indirect confirmation of this assumption was obtained in the experiments on magnetic susceptibility in the series of phases $CeNi_2B_2C$, $NdNi_2B_2C$, and $GdNi_2B_2C$.[175, 176]

X-Ray absorption spectra of $Y_{1-x}Ce_xNi_2B_2C$ alloys ($x = 0$, 0.05, 0.1, 0.25, and 1.0) were obtained in the energy region 5680 – 5820 eV corresponding to the L_{III} edge of Ce absorption at 300 and 10 K. The absorption spectrum contains two resolved peaks at $E \simeq 5723$ and 5731 eV assigned to the Ce4f^1 and Ce4f^0 configurations, respectively. The relative intensities of these maxima change with temperature, which directly indicates a fluctuation of the valence state of cerium. Decomposition of spectral lines into individual components according to the procedure suggested [177, 178] makes it possible to estimate the averaged cerium valence ($\langle \upsilon \rangle$). The $\langle \upsilon \rangle$ values obtained 3.15 and 3.21 (at $T = 300$ K and 10 K, respectively) are smaller than 3.33, which is usually obtained for the ions with a formal valence of 4 by the XAS method. The standard underestimation of $\langle \upsilon \rangle$ as compared to the value of the formal valence is due to the final state effect.[179] In $Y_{1-x}Ce_xNi_2B_2C$ solid solutions, cerium also has a variable valence ($\langle \upsilon \rangle = 3.18$). It is of interest to note that the $\langle \upsilon \rangle$ value decreases at elevated temperature and increases at low temperature ($T = 10$ K) as the cerium concentration in the solid solution increases. Alleno *et al.*[174] explained the distinctions in the temperature dependence of $\langle \upsilon \rangle$ for Ce in $CeNi_2B_2C$ and $Y_{1-x}Ce_xNi_2B_2C$ solid solutions diluted with respect to Ce by co-operative effects.[177]

Additional information on the valence states of Ce can be obtained using the X-ray fluorescence spectroscopy of core levels.

IX. Conclusion

Over a rather short period elapsed from the beginning of intensive studies of IBC, a considerable body of information on the physicochemical properties of this group of compounds has been accumulated. The available data are dissimilar. Intermetallic borocarbides are a unique class of multicomponent superconducting magnetic materials. For this reason, their low-temperature electrophysical and magnetic characteristics have been studied in most detail.

Much less information on phase equilibria and phase diagrams of IBC is available, while their thermodynamic and thermomechanical properties have not virtually been studied. The latter is also true for the problems of targeted synthesis of IBC and the effect of various structural defects on the properties of these compounds. A systematic accumulation of information on the above lines is required to develop the fundamentals of material science of IBC.

Only the principal results of the studies of the electronic structure of intermetallic borocarbides have been covered in this review. Currently, prominent specific features of electron distributions and chemical bonding in IBC have been reliably established. The mechanism of the formation of several physicochemical properties of these compounds has been explained from the viewpoint of their electronic structure.

It should be noted that most of the available data refer to nonexcited electronic subsystems of ideal quaternary phases in the nonmagnetic state. Taking account of a swift increase in the experimental information on the properties of IBC, particular attention of theoreticians in the near future will most likely be drawn to describing the microscopic nature of the origin of magnetic order, conditions of its coexistence with superconductivity, relationship between the superconductivity and the valence state of lanthanides, possible external effects (pressure or temperature) on the spin subsystems.

Setting up research in the field of theoretical material science of IBC associated with problems of constructing phase and magnetic phase diagrams, computer simulation of new multicomponent phases, their solid solutions, studies of the influence of various impurities and structural defects on the properties of IBC appears to be no less urgent.

References

1. R J Cava, H Takagi, B Batlogg, H W Zandbergen, J J Krajewski, W F Peck, R van Dover, R J Felder, T Siegrist, T K Mizuhashi, J O Lee, H Eisaki, S A Carter, S Uchida *Nature* (*London*) **367** 146 (1994)
2. R J Cava, H Takagi, H W Zandbergen, J J Krajewski, W F Peck, T Siegrist, B Batlogg, H W Zandbergen, R van Dover, R J Felder, K Mizuhashi, J O Lee, H Eisaki, S Uchida *Nature* (*London*) **367** 252 (1994)
3. R Nagarajan, C Mazumdar, Z Nossian, S K Dhar, K V Gopalakrishnan, L C Gupta, C Godart, B D Padalia, R Vijayaraghavan *Phys. Rev. Lett.* **72** 274 (1994)
4. S V Vonsovskii, Yu A Izyumov, E Z Kurmaev *Sverkhprovodimost' Perekhodnykh Metallov, Ikh Splavov i Soedinenii* (Superconductivity of Transition Metals and Their Alloys and Compounds) (Moscow: Nauka, 1977)
5. W H Lee, F A Yang, C R Shin, H D Yang *Phys. Rev. B, Condens. Matter* **50** 6523 (1994)
6. W H Lee, H K Zeng, Y D Yao, Y Y Chen *Physica C* **226** 138 (1996)
7. W H Lee, H K Zeng *Solid State Commun.* **101** 323 (1997)
8. H Schmidt, M Muller, U F Braun *Phys. Rev. B, Condens. Matter* **53** 12389 (1996)
9. T Siegrist, H W Zandbergen, R J Cava, J J Krajewski, W F Peck *Nature* (*London*) **367** 254 (1994)
10. H Eisaki, H Takagi, R J Cava, K Mizuhashi, J O Lee, B Batlogg, J J Krajewski, F Peck, S Ushida *Phys. Rev. B, Condens. Matter* **50** 647 (1994)
11. B K Cho, M Xu, P C Canfield, L L Miller, D C Johnston *Phys. Rev. B, Condens. Matter* **53** 3676 (1995)
12. B K Cho, P C Canfield, L L Miller, D C Johnston, W P Beyermann, A Yatskar *Phys. Rev. B, Condens. Matter* **52** 3684 (1995)
13. K D Rathnayaka, D G Naugle, B K Cho, P C Canfield *Phys. Rev. B, Condens. Matter* **53** 5688 (1996)
14. B K Cho, P C Canfield, D C Johnston *Phys. Rev. B, Condens. Matter* **52** R3844 (1995)
15. R J Cava, B Batlogg, T Siegrist, J J Krajewski, W F Peck, S Carter, R J Felder, H Takagi, R van Dover *Phys. Rev. B, Condens. Matter* **49** 12 384 (1994)
16. H W Zandbergen, R J Cava, J J Krajewski, W F Peck *Physica C* **230** 6 (1994)
17. Y Y Sun, I Rusakova, R L Meng, Y Cao, P Gautier-Picard, C W Chu *Physica C* **230** 435 (1994)
18. A K Gangopadhyay, A J Schuetz, J S Schilling *Physica C* **246** 317 (1995)
19. A I Goldman, C Stassis, P C Canfield, S Zarestky, P Dervenages, B K Cho, D C Johnston, B Sternlieb *Phys. Rev. B, Condens. Matter* **50** 9668 (1994)
20. T E Grigereit, J W Lynn, Q Huang, A Santoro, R J Cava, J J Krajewski, W F Peck *Phys. Rev. Lett.* **73** 2756 (1994)
21. S K Sinha, J W Lynn T E Grigereit, Z Hossain, L C Gupta, R Nagarajan, C Godart *Phys. Rev. B, Condens. Matter* **51** 681 (1995)
22. J Zarestky, C Stassis, A I Goldman, P C Canfield, P Dervenagas, B K Cho, D C Johnston *Phys. Rev. B, Condens. Matter* **51** 678 (1995)
23. P Dervenagas, J Zarestky, C Stassis, A I Goldman, P C Canfield, B K Cho *Physica B* **212** 1 (1995)
24. P C Canfield, B K Cho, K W Dennis *Physica B* **215** 337 (1995)
25. C Detlefs, A I Goldman, C Stassis, P C Canfield, B K Cho, J P Hill, D Gibbs *Phys. Rev. B, Condens. Matter* **53** 6355 (1996)
26. T Takabatake, Y Maeda, T Konishi, H Fuji *J. Phys. Soc. Jpn.* **63** 2853 (1994)
27. Z Hossain, L C Gupta, R Nagarajan, P Raj, S Dhar, C Godart, P Suryanarayana, S N Bagchi, V G Date, D C Purushotham, R Vijayaraghavan *Europhys. Lett.* **28** 55 (1994)

28. H W Zandbergen, E J van Zwet, J Sarrac, M de Andrade, J Hermann, S H Han, Z Fisk, M B Maple, R J Cava *Physica C* **229** 29 (1994)
29. M Vybornov, H Noel, P Boulet, P Rogl, in *Proceedings of the 12th International Symposium on Boron, Borides, Related Compounds* (*ISNN 96*) (*Abstracts of Reports*) (Vienna: Vienna University, 1996) p. 46
30. R Krendelsberger, P Rogl, H Michor, G Hilscher, E Bauer, C Dusek, R Hauser, L Naber, D Werner, H W Zandberger, in *Proceedings of the 12th International Symposium on Boron, Borides, Related Compounds* (*ISNN 96*) (*Abstracts of Reports*) (Vienna: Vienna University, 1996) p. 105
31. G Hilscher, H Michor, E Bauer, C Dusek, R Hanser, L Naber, D Werner, R Krendelsberger, P Rogl, H W Zandberger, in *Proceedings of the 12th International Symposium on Boron, Borides, Related Compounds* (*ISNN 96*) (*Abstracts of Reports*) (Vienna: Vienna University, 1996) p. 42
32. S L Bud'ko, M ElMassalami, M B Fontes, J Mondragon, W Vanoni, B Giordanengo, E M Baggio-Saitovitch *Physica C* **243** 183 (1995)
33. S L Bud'ko, M B Fontes, D Aliaga-Guerra, E M Baggio-Saitovich *Phys. Rev. B, Condens. Matter* **52** 305 (1995)
34. A K Gangopadhyay, J S Schilling *Physica C* **264** 281 (1996)
35. H Fujii, T Kimura, K Hirata, T Mochiku, H Kumakura, K Togano *Physica C* **256** 143 (1996)
36. X D Qiu, L Gao, R L Meng, Y Y Sun, Y Y Xue, C W Chu *Phys. Rev. B, Condens. Matter* **53** 12 318 (1996)
37. A K Gangopadhyay, J S Schilling *Phys. Rev. B, Condens. Matter* **54** 10 107 (1996)
38. P Vilars, L D Calvert *Pearson's Handbook of Crystallographic Data for Intermetallic Phases* (New York: Int. Mat. Park. ASM, 1991)
39. H C Ku, C C Lai, Y B You, J H Shieh, W Y Guan *Phys. Rev. B, Condens. Matter* **50** 351 (1994)
40. R J Cava, T Siegrist, B Batlogg, H Takagi, H Eisaki, S A Carter, J J Krajewski, W E Peck *Phys. Rev. B, Condens. Matter* **50** 12 966 (1994)
41. L Gao, X D Qiu, Y Cao, R L Meng, Y Y Sun, Y Y Xue, C W Chu *Phys. Rev. B, Condens. Matter* **50** 9445 (1994)
42. X D Qiu, L Gao, Y Y Xue, C W Chu *Bull. Am. Phys. Soc.* **40** 627 (1995)
43. R D Shannon, C T Prewitt *Acta Crystallogr., Sect. B* **26** 1046 (1970)
44. A Iandelli, A Palenzona, in *Handbook of the Physics and Chemistry of Rare Earths* (Eds K A Gshneider, L Eyring) (Amsterdam: North-Holland, 1984)
45. L C Gupta, R Nagarajan, Z Hossain, C Mazumdar, S K Dhar, C Godart, C Levy-Clement, B D Padalia, R Vijayaraghavan *J. Magn. Magn. Mater.* **140 – 144** 2053 (1995)
46. M ElMassalami, S L Bud'ko, B Giordanengo, E M Baggio-Saitovitch *Physica C* **224** 41 (1995)
47. J W Lynn, S Skanthakumar, Q Huang, S K Sinha, Z Hossian, L C Gupta, R Nagarajan, C Godart *Phys. Rev. B, Condens. Matter* **55** 6584 (1997)
48. F J Disalvo *Science* **247** 649 (1992)
49. T H Geballe *Science* **259** 1550 (1993)
50. L F Mattheiss *Phys. Rev. B, Condens. Matter* **49** 13 279 (1994)
51. L F Mattheiss, D R Hamann *Phys. Rev. B, Condens. Matter* **33** 823 (1986)
52. O K Andersen *Phys. Rev. B, Solid State, Ser. 3* **12** 3060 (1975)
53. E Wigner *Phys. Rev.* **46** 1002 (1934)
54. L F Mattheiss *Phys. Rev. Lett.* **58** 1028 (1987)
55. B M Klein, L L Boyer, D A Papaconstantopoulos, L F Mattheiss *Phys. Rev. B, Condens. Matter* **18** 6411 (1978)
56. B Batlogg, in *Mechanism of High Temperature Superconductivity* (Eds A Kamimura, A Oshiyama) (Berlin: Springer, 1989) p. 324
57. S A Carter, B Batlogg, R J Cava, J J Krajewski, W F Peck, H Takagi *Phys. Rev. B, Condens. Matter* **50** 4216 (1994)
58. L F Mattheiss *Phys. Rev. B, Condens. Matter* **47** 8224 (1993)
59. W F Pickett, D J Singh *Phys. Rev. Lett.* **72** 3702 (1994)
60. S H Wei, H Krakauer *Phys. Rev. Lett.* **55** 1200 (1985)
61. D Singh *Planewaves. Pseudopotentials and the LAPW Method* (Boston: Kluwer Academic, 1994)
62. D Singh *Phys. Rev. B, Condens. Matter* **43** 6388 (1991)
63. S Vosko, P Wilk, S H Nusiar *Can. J. Phys.* **58** 1200 (1980)
64. L F Mattheiss, T Siegrist, R J Cava *Solid State Commun.* **91** 587 (1994)
65. K Schwarz, P Mohn *J. Phys. F, Met. Phys.* **14** L129 (1984)
66. A Williams, J Moruzzi, J Kubler, K Schwarz *Bull. Am. Phys. Soc.* **29** 278 (1984)
67. V A Gubanov, E Z Kurmaev *Zh. Strukt. Khim.* **29** 143 (1988) [a]
68. H Kim, C-D Hwang, J Ihm *Phys. Rev. B, Condens. Matter* **52** 4592 (1995)
69. J Ihm, A Zunger, M L Cohen *J. Phys. C, Solid State Phys.* **12** 4409 (1979)
70. R Coehoorn *Physica C* **228** 331 (1994)
71. J I Lee, T S Zhao, I G Kim, B I Min, S J Youn *Phys. Rev. B, Condens. Matter* **50** 4030 (1994)
72. P Ravindran, S Sankaralingam, R Asokamani *Phys. Rev. B, Condens. Matter* **52** 12 921 (1995)
73. Z Zeng, D E Ellis, D Guenzburger, E M Baggio-Saitovitch *Phys. Rev. B, Condens. Matter* **53** 6613 (1996)
74. N M Hong, H Michor, M Vybornov, T Holubar, P Hundegger, W Perthold, G Hilscher, P Rogl *Physica C* **227** 85 (1994)
75. R J Hoffmann *Rev. Mod. Phys.* **60** 601 (1988)
76. C D Gelatt, A R Williams, V L Moruzzi *Phys. Rev. B, Condens. Matter* **27** 2005 (1983)
77. J-F Halet *Inorg. Chem.* **33** 4173 (1994)
78. R J Hoffmann *Chem. Phys.* **39** 1397 (1963)
79. M-H Whangbo, R J Hoffmann *J. Am. Chem. Soc.* **100** 6093 (1978)
80. D E Ellis *Int. J. Quantum Chem., Suppl.* **2** 35 (1968)
81. D E Ellis, G S Painter *Phys. Rev. B, Solid State, Ser. 3* **2** 2887 (1970)
82. B Delley, D E Ellis *J. Chem. Phys.* **76** 1949 (1982)
83. D E Ellis, G Benesch, E Byrom *Phys. Rev. B, Solid State, Ser. 3* **16** 3308 (1977)
84. P L Cao, D E Ellis, A J Freeman *Phys. Rev. B, Condens. Matter* **25** 2124 (1982)
85. D E Ellis, J Guo, J J Low, in *Quantum Chemistry Approach to Chemosorption and Heterogeneous Catalysis* (Ed. F Ruette) (Amsterdam: Kluwer Academic, 1992)
86. U van Barth, L Hedin *J. Phys. C, Solid State Phys.* **5** 1629 (1972)
87. D J Singh *Phys. Rev. B, Condens. Matter* **50** 6486 (1994)
88. B M Klein, W E Pickett, in *Superconductivity in d- and f-Band Metals* (Eds W Buckel, W Weber) (Karlsruhe: Kernforsch und Karlsruhe GmbH, 1982) p. 477
89. A R Williams, J Kubler, C D Gelatt *Phys. Rev. B, Condens. Matter* **19** 6094 (1979)
90. H Schmidt, M Muller, H F Braun *Physica C* **235 – 240** 779 (1994)
91. A B Kaiser, *J. Phys. C* **3** 410 (1970)
92. M B Maple, in *Magnetism* Vol. 5 (Eds G Rado, H Suhl) (New York: Academic Press, 1973) p. 289
93. Y Xue *Solid State Commun.* **68** 395 (1988)
94. H Schmidt, H F Braun *Physica C* **229** 315 (1994)
95. B C Chakoumakos, M Paranthaman *Physica C* **227** 143 (1994)
96. D Lide (Ed.) *CRC Handbook of Chemistry and Physics* (Boca Raton, FL: CRC Press, 1991)
97. C C Hoellworth, P Klavins, R N Shelton *Phys. Rev. B, Condens. Matter* **53** 2579 (1996)
98. K Kadowaki, H Takeya, K Hirata, T Mochiku *Physica B* **206 – 208** 555 (1995)
99. S B Roy, Z Hossian, A K Prodhan, P Chhaddah, R Nagarajan, L C Gupta *Physica C* **256** 90 (1996)
100. B Suh, F Borsa, D R Torgeson, B Cho, P C Canfield, D C Johnston, J Y Rhee, B N Harmon *Phys. Rev. B, Condens. Matter* **53** R6022 (1996)
101. T Kohara, T Oda, K Ueda, Y Yamada, A Mahajan, E Elankumaran, Z Hossian, L C Gupta, R Nagarajan, R Vijayraghavan, C Majumdar *Phys. Rev. B, Condens. Matter* **51** 3985 (1995)
102. K Ikushima, J Kickuchi, H Yasuoka, R J Cava, H Takagi, J J Krajewski, W W Peck *J. Phys. Soc. Jpn.* **63** 2878 (1994)
103. K Prassides, A Lappas, M Buchgeister, P Vergas *Europhys. Lett.* **29** 641 (1995)
104. H Michor, T Holubar, C Dusek, G Hilscher *Phys. Rev. B, Condens. Matter* **52** 16 165 (1995)
105. C Looney, A K Gangopadhaya, A K Klehe, J S Schilling *Physica C* **252** 199 (1995)
106. P W Anderson *Phys. Chem. Solids* **11** 26 (1995)

107. *Transport and Thermal Properties of f-Electron Systems* (Ed. G Oomi) (New York: Plenum, 1993)
108. D D Lawrie, J P Frank *J. Supercond.* **8** 591 (1995)
109. M Xu, P C Canfield, J E Ostenson, D K Finnemore, B K Cho, Z R Wang, D C Johnston *Physica C* **227** 321 (1994)
110. P Dervenagas, M Bullock, J Zarestky, P Canfield, B K Cho, B Harmon, A J Goldman, C Stassis *Phys. Rev. B, Condens. Matter* **52** R9839 (1995)
111. H Kawano, H Yoshizawa, H Takeya, K Kadowaki *Phys. Rev. Lett.* **77** 4629 (1996)
112. F Bommeli, L Degiordi, P Wachter, B K Cho, P C Canfield, R Chau, M B Maple *Phys. Rev. Lett.* **78** 547 (1997)
113. K Widder *Europhys. Lett.* **30** 55 (1995)
114. I K Yanson, V V Fisun, A G Jansen, P Wyder, P C Canfield, B K Cho, C V Tomy, D Paul *Phys. Rev. Lett.* **78** 935 (1997)
115. A V Khotkevich, I K Yanson *Atlas of Point Contact Spectra of Electron-Phonon Interactions in Metals* (New York: Kluwer Academic, 1995)
116. M B Maple, O Fischer (Eds) *Superconductivity in Ternary Compounds* Vol. II (Berlin: Springer, 1982)
117. P C Canfield, B K Cho, D C Johnston, D K Finnemore, M F Hundley *Physica C* **320** 397 (1994)
118. M S Lin, J H Shieh, Y B Yon, W Y Guan, H C Ku, H D Yang, J C Ho *Phys. Rev. B, Condens. Matter* **52** 1181 (1995)
119. M El Massalami, E M Baggio-Saitovitch *J. Magn. Magn. Mater.* **153** 97 (1996)
120. Q Huang, A Santoro, T B Grigereit, J W Lynn, R J Cava, J J Krajewski, W F Peck *Phys. Rev. B, Condens. Matter* **51** 3701 (1995)
121. T E Grigereit, J W Lynn, R J Cava, J J Krajewski, W F Peck *Physica C* **248** 382 (1995)
122. C V Tomy, L J Chang, D McPaul, N H Andersen, M Yethiraj *Physica B* **213**–**214** 139 (1995)
123. J W Lynn, Q Huang, A Santoro, R J Cava, J J Krajewski, W F Peck *Phys. Rev. B, Condens. Matter* **53** 802 (1996)
124. B K Cho, B N Harmon, C D Johnston, P C Canfield *Phys. Rev. B, Condens. Matter* **53** 2217 (1996)
125. D R Sanchez, H Micklitz, M B Fontes, S L Bud'ko, E Baggio-Saitovitch *Phys. Rev. Lett.* **76** 507 (1996)
126. J P Hill, B J Sternlieb, D Gibbs, C Detlefs, A I Goldman, C Stassis, P C Canfield, B K Cho *Phys. Rev. B, Condens. Matter* **53** 3487 (1996)
127. J W Lynn, Q Huang, S K Sinha, Z Hossain, L C Gupta, R Nagarajan, C Godart *Physica C* **224** 66 (1996)
128. C V Tomy, L J Chang, D McPaul, N H Andersen, M Yethiraj *Physica B* **224** 116 (1996)
129. C V Tomy, G Balakrishnan, D McPaul *Physica C* **248** 349 (1995)
130. M S Lin, J H Shieh, Y B You, Y Y Hsu, J W Chen, S H Lin, Y D Yao, J C Ho, H C Ku *Physica C* **249** 403 (1995)
131. C V Tomy, M R Lees, L Afalfiz, G Balakrishnan, D McPaul *Phys. Rev. B, Condens. Matter* **52** 9186 (1995)
132. Z Hossain, R Nagarajan, L C Gupta, S K Dhar, C Godart, R Vhijayaraghavan *Physica B* **223**–**224** 99 (1996)
133. P Dervenagas, J Zarestky, C Stassis, A I Goldman, P C Canfield, B K Cho *Phys. Rev. B, Condens. Matter* **53** 8506 (1996)
134. B K Cho, P C Canfield, D C Johnston *Phys. Rev. B, Condens. Matter* **53** 8499 (1996)
135. C V Tomy, L A Afalfiz, M R Lees, J M Martin, D McPaul, D T Adroja *Phys. Rev. B, Condens. Matter* **53** 307 (1996)
136. J W Lynn, Q Huang, S K Sinha, Z Hossian, L C Gupta, R Nagarajan, C Godart *J. Appl. Phys.* **79** 5857 (1996)
137. L J Chang, C V Tomy, D McPaul, C Ritter *Phys. Rev. B, Condens. Matter* **54** 9031 (1996)
138. D W Cooke, J L Smith, S J Blundell, K H Chow, P A Pattenden, F L Pratt, S F Cox, S R Brown, A Morrobel-Sosa, R L Lichti, L C Gupta, R Nagarajan, Z Hossain, C Mazumdar, C Goddart *Phys. Rev. B, Condens. Matter* **52** R3864 (1995)
139. S K Dhar, R Nagarajan, Z Hossain, C Godart, L C Gupta, R Vijayaraghavan *Solid State Commun.* **98** 985 (1996)
140. H Schmidt, M Weber, H F Braun *Physica C* **246** 117 (1995)
141. H Schmidt, M Weber, H F Braun *Physica C* **256** 393 (1996)
142. W A Fertig, D C Johnston, L E Delong, R W McCallum, M B Maple, B T Mattias *Phys. Rev. Lett.* **38** 987 (1977)
143. M Ishikawa, O Fischer *Solid State Commun.* **23** 37 (1977)
144. J Y Rhee, X Wang, B N Harmon *Phys. Rev. B, Condens. Matter* **51** 15 585 (1995)
145. V S Grechishkin *Yadernye Kvadrupol'nye Vzaimodeistviya v Tverdykh Telakh* (Nuclear Quadrupole Interactions in Solids) (Moscow: Nauka, 1973)
146. N N Grenwood, T C Gibbs *Mössbauer Spectroscopy* (London: Chapman and Hall, 1971)
147. R Coehoorn, K H Buschow, M W Dirken, R C Thiel *Phys. Rev. B, Condens. Matter* **42** 4645 (1990)
148. F M Mulder, J H Brabers, R Coehoorn, R C Thiel, K H Buschow, F R de Boer *J. Alloys Compd.* **217** 118 (1995)
149. G J Long, R Kulasekere, O A Pringle, F Grandjean, K H Buschow *J. Magn. Magn. Mater.* **117** 239 (1992)
150. M W Dirken, R C Thiel, R Coehoorn, T H Jacobs, K H Buschow *J. Magn. Magn. Mater.* **94** L15 (1991)
151. R Coehoorn, G H Daalderop *J. Magn. Magn. Mater.* **104**–**107** 1081 (1992)
152. P C Gubbenes, A A Moolenaar, T H Jacobs, K H Bischow *J. Alloys Compd.* **176** 115 (1991)
153. J Terra, D Guenzburger *Phys. Rev. B, Condens. Matter* **44** 1611 (1991)
154. D Guenzburger, D E Ellis *Phys. Rev. B, Condens. Matter* **36** 6971 (1987)
155. A L Ivanovskii, V P Zhukov, V A Gubanov *Elektronnoe Stroenie Tugoplavkikh Karbidov i Nitridov Perekhodnykh Metallov* (Electronic Structure of High-Melting Carbides and Nitrides of Transaction Metals) (Moscow: Nauka, 1990)
156. V P Zhukov *Zh. Strukt. Khim.* **38** 554 (1997) [a]
157. P Vinet, J H Rose, J Ferrante, J R Smith *J. Phys., Condens. Matter.* **1** 1941 (1989)
158. P Vinet, J Ferrante, J R Smith, J H Rose *J. Phys. C, Solid State Phys.* **19** 9319 (1987)
159. M S Golden, M Knupfer, M Kielwein, M Buchdeister, J Fink, D Teehan, W E Pickett, D J Singh *Europhys. Lett.* **28** 369 (1994)
160. A Fujimori, K Kobayashi, T Mizokawa, K Mamiya, A Sekiyama, H Easaki, H Takagi, S Uchida, R J Cava, J J Krajewski, W F Peck *Phys. Rev. B, Condens. Matter* **50** 9660 (1994)
161. J J Yeh, I Lindau *At. Data Nucl. Data Tables* **32** 1 (1983)
162. D R Penn *Phys. Rev. Lett.* **42** 921 (1979)
163. L C Davis, L Feldkamp *Solid State Commun.* **34** 141 (1980)
164. W Eberhard, E W Plummer *Phys. Rev. B, Condens. Matter* **21** 3245 (1980)
165. G A Sawatzky, J W Allen *Phys. Rev. Lett.* **53** 2339 (1984)
166. A Fujimori, F Minami *Phys. Rev. B, Condens. Matter* **30** 957 (1984)
167. K Ho, M L Cohen, W E Pickett *Phys. Rev. Lett.* **41** 815 (1978)
168. M Vekic, S R White *Phys. Rev. B, Condens. Matter* **48** 7643 (1993)
169. A Kampf, J R Schieffer *Phys. Rev. B, Condens. Matter* **41** 6339 (1990)
170. A Fujimori, K Kobajashi, T Mizokawa, K Mamiya, A Sekiayama, H Takagi, H Easaki, S Uchida, R J Cava, J J Krajewski, W F Peck *J. Phys. Chem. Solids* **56** 1875 (1995)
171. J Guo, Ph. Thesis, Uppsala University, Uppsala, 1995
172. S Shin, A Agui, M Watanabe, M Fujisawa, Y Tezuka, T Ishii, K Kobayashi, A Fujimori, M Hinomaru, H Takagi *Phys. Rev. B, Condens. Matter* **52** 15 082 (1995)
173. E Pellegrin, C T Chen, G Meigs, R J Cava, J J Krajewski, W F Peck *Phys. Rev. B, Condens. Matter* **51** 16 159 (1995)
174. E Alleno, Z Hossain, C Godart, R Nagarajan, L C Gupta *Phys. Rev. B, Condens. Matter* **52** 7428 (1995)
175. R Nagarajan, L C Gupta, S K Dhar, C Mazumdar, Z Hossain, C Godart, C Levy-Chement, B D Padalia, R Vijayaraghavan *Physica B* **206**–**207** 548 (1994)
176. L C Gupta, R Nagarajan, C Godart, S K Dhar, C Mazumdar, Z Hossain, C Levy-Chement, B D Padalia, R Vijayaraghavan *Physica C* **235**–**240** 150 (1994)
177. M Groff, J A Hodges, E Kemly, A Krishnan, V Murgai, L C Gupta *Phys. Rev. Lett.* **48** 826 (1982)
178. N B Brandt, V V Moschalkov *Adv. Phys.* **33** 373 (1994)
179. G Krill, J P Kappler, A Meyer, L Abadi, M F Ravet *J. Phys. (France)* **11** 1713 (1981)

[a] — *J. Struct. Chem. (Engl. Transl.)*